Uncertainty Propagation in Flutter Analysis

RESEARCH · SEPTEMBER 2015

DOI: 10.13140/RG.2.1.3116.5920

1 AUTHOR:

Jan Schwochow

German Aerospace Center (DLR)

35 PUBLICATIONS **7** CITATIONS

Uncertainty Propagation in Flutter Analysis

Jan Schwochow

DLR Göttingen

jan.schwochow@dlr.de

Contents

Nomenclature

Physical variables

$[AIC]$	aerodynamic coefficient matrix
a_∞	speed of sound
$[B]$	expanded mode shape matrix
$[C_{hh}]$	modal mass matrix
$\{c_p\}$	vector pressure coefficients
c	reference length
$[F]$	aeroelastic coefficient matrix (flutter matrix)
h	increment step size
$[K]$	physical stiffness matrix
$[K_{hh}]$	modal stiffness matrix
$k = \frac{\omega c}{V_\infty}$	reduced frequency
$[M]$	physical mass matrix
$[M_{hh}]$	modal mass matrix
M_∞	freestream Mach number
$[Q_{hh}]$	modal aerodynamic load matrix
$\{q\}$	modal participation vector
$[S]$	sign matrix
$s = \sigma + i\omega$	Laplace variable
$[T]$	transformation matrix between structural and aerodynamic mesh
$\{\Delta u\}$	vector of uncertain structural parameters
V_∞	freestream velocity
$[w]$	downwash matrix
$\{x\}$	vector of displacements
$\{\dot{x}\}$	vector of velocities

$\{\ddot{x}\}$	vector of accelerations
$[\Phi] = \left[\{\phi_1\} \quad \{\phi_2\} \quad \dots \quad \{\phi_m\}\right]$	matrix of mode shapes
$\{\psi\}$	reduced mode shape vector
$[\Lambda]$	diagonal matrix of eigenvalues
λ	eigenvalue
ρ_∞	air density
ω	eigen frequency

Matrix notation

$\{\dots\}$	column vector
$[\dots]$	matrix
$[\dots]^T$	transpose of matrix
$[\dots]^{-1}$	inverse of matrix

Operators

$\underline{x}$	lower bound
$\overline{x}$	upper bound
x^C	centered value
Δx	uncertain or radius value

Indices

a	aerodynamic
s	structural

Tables

Figures

1 Introduction

Flutter is a self-excited vibration that can occur with elastic structures that are subject to airflow when the interaction of deflection and the induced air forces transmit energy from the flow into the oscillation of the structure. This may lead to damage or destruction of the vibrating structure. The examination of the dynamic stability of an aircraft requires the exact determination of the elastic behaviour, structural damping and inertia forces, as well as the aerodynamic forces in connection with the matched point flow parameters. For this purpose, suitable simulation models are set up that must be validated by experiments. Since simplifications are introduced in the theoretical formation of the models on one hand, and the measuring accuracy is limited in the experiment on the other, models and their parameters may include uncertainties, making it difficult to determine the dynamic stability boundaries. For the robust flutter analysis, it is necessary to propagate the effects of identified uncertainties towards aeroelastic stability of the aircraft to cover the uncertain-but-bounded parameter space. Robust stability is guaranteed when the uncertainties cannot destabilize the system. In recent years, the so-called μ-analysis from the control community has been applied to perform robust flutter analysis [11]. Borglund formulated the μ-k method [4], where the classical frequency-domain aeroelasticity of p-k and g methods ([10], [6]) are combined with μ-analysis. In this paper, a combined method is proposed which determines the lower and upper bounds of eigen frequencies and mode shapes by the non-probabilistic interval modal analysis method from Sim and Qiu [16]. Then these bounds are tracked through the flutter stability analysis by applying the continuation method from Cardani and Mantegazza [5]. Each modal degree of freedom DoF is continued for increasing flight velocity. After each continuation step, the bounds of aeroelastic damping and frequency are evaluated.

2 Uncertainties in robust flutter analysis

For an efficient and reliable aeroelastic certification process, the uncertainties in the aerodynamic and structural dynamic modelling must be estimated in order to decide whether they can be tolerated or must be push under an uncritical threshold value. The analysis must look for the most unfavourable combination of the essential parameters (worst case) in order to ensure safe operation in the entire flight envelope.

The stability analysis assumes that the vibration of the airplane in free flight is composed of rigid body modes, vibration modes of the airframe and deflection of control surfaces through linear superposition. The eigen frequencies and mode shapes can be determined during the design process through modal analysis based on the finite element method. It is generally necessary, however, before the first flight, to check the structural models of the airplane by conducting a ground vibration test on the first prototype. Possible deviations between the model and experiment reflect the structural dynamic uncertainties for the ensuing proof of stability. For small airplanes, structural dynamic models are often not available, so that one must solely rely upon the measured modal data including measurement noise.

The numerical modelling of structural dynamics of the aircraft is based on simplifications of the actual structure and is conducted in connection with parameters that determine geometry, material characteristics and boundary conditions. The determining physical parameters include uncertainties, whose causes can be divided as follows:

Intentional simplifications: Individual dynamic effects are rendered simplified because the expenditure of possible refinement is disproportionate to the resulting improvement. For example, the dynamic modelling of the mechanical or hydraulic control system of an airplane is simplified to an equivalent system of spring and damping elements.

Dynamics that are unknown or cannot be modelled: This group comprises of dynamic features that influence the system behaviour, but are unknown. Friction or free-play in the airplane structure or in the control system can often not be represented in FE-models. Furthermore, the vibration modes are usually only determined on the unstressed airplane.

Parameter uncertainties: Even if the model renders physically correct the individual influences, quantitative inaccuracies can still result in parametric uncertainties. For example, the modulus of elasticity is dependent on the load path, especially in composite components.

Stochastic uncertainty factors: This group consists of uncertainties that overlap in reality and therefore can never be exactly determined. Due to production inaccuracies, the modulus of elasticity varies for bolt and rivet joints for example. The resin to fibre ratio influences the weight of the composite components. For experimental data, measurement noise generally shows stochastic nature.

To ensure flutter-free operation of the aircraft it is convenient to describe the identified structural uncertainties as perturbation parameters based on a nominal model. Different approaches can be applied to determine the deviation of the nominal model. The methods can be distinguished in probabilistic and non-probabilistic concepts. In Monte Carlo simulations [13] a random generator fills the vector of the uncertainty parameters, the system matrices are evaluated, and the modal analysis problem is solved. In order to obtain a statistically funded statement, many random combinations must be analysed. Therefore, this procedure requires a high amount of computational work, but can be easily integrated into an existing process. In the selection of the probability distribution for each entry, the state of knowledge of the variations of the parameters is reflected that is gained through experience or statistical evaluations. When determining the flutter stability for the certification of a new aircraft design, it must be assured that there is no danger of flutter for all combinations of the uncertain parameters up to the interval boundaries. For the non-probabilistic propagation of uncertain-but-bounded parameters in modal analysis, deterministic interval methods ([15], [16]) can calculate upper and lower bounds of natural frequencies and modal shapes in an efficient manner. For further decrease of the computational costs, transformation to adequate subspaces reduces the full order model in physical DoF to significantly lower orders. An expanded modal matrix approximates the vibration mode shapes of the modified structure using the nominal eigenvectors and their sensitivities with respect to the uncertain parameters or using families of eigenvectors calculated from the lower and upper bounds of the identified uncertain parameters.

In order to evaluate aeroelastic stability boundaries the established procedures for

the solution of the flutter equations according to the p-k method [10] and the g-method [6] respectively must be expanded so that the dependencies of the stability towards upper and lower bounds of frequencies and modal shapes can be described. Although the flutter equations are formulated in modal DoF, the unsteady air loads depend upon the uncertainties in spatial distributions of modal deflections. In commercial aeroelastic codes, such as NASTRAN [18] or ZAERO [17], the stability analysis is conducted for the entire deterministic system with all DoF. The modified system requires a completely new calculation. As an alternative in [5] and [14], the continuation method is suggested for the solution of the flutter equations. The non-linear system of flutter equations are solved in a direct manner for a free continued parameter. One single solution branch is tracked for increasing flight speed using a predictor-corrector procedure. For this purpose, the continuation method requires starting solutions, which are the modal results at zero flight speed. The advantage is seen in the specific stability examination of individual critical solution branches, which are active in the identified flutter mechanism without reduction or truncation of the entire system. In [12] the continuation method is used to analyse the effect of structural non-linearities in the flutter analysis caused by free-play, so that the critical flutter speeds are dependent on the amplitude of control surface deflections.

3 Direct solution of flutter equations

The flutter equations are generally set up in modal DoF. in the Laplace-domain:

$$\left(\left[M_{hh} \right] s^2 + \left[C_{hh} \right] s + \left[K_{hh} \right] - \frac{1}{2} \rho_\infty V_\infty^2 \left[Q_{hh} \left(M_\infty, k \right) \right] \right) \{q\} = \{0\}, \tag{1}$$

where $\left[M_{hh} \right] = \left[\Phi \right]^T \left[M \right] \left[\Phi \right]$ is the generalized inertia matrix, $\left[C_{hh} \right] = \left[\Phi \right]^T \left[C \right] \left[\Phi \right]$ is the generalized damping matrix, $\left[K_{hh} \right] = \left[\Phi \right]^T \left[K \right] \left[\Phi \right]$ is the generalized stiffness matrix and $\left[Q_{hh} \left(M_\infty, k \right) \right]$ is the generalized aerodynamic loading matrix. The latter non-linearly depends on the Mach number M_∞ and the reduced frequency k, defined in the following way:

$$k = \frac{\omega c}{V_\infty} = \frac{\mathrm{Im}(s) c}{V_\infty}, \tag{2}$$

where c is a specified reference length and V_∞ is the true undisturbed freestream velocity. The aerodynamic force matrix is pre-multiplied by the dynamic pressure, so that it depends quadratically on the freestream velocity and linearly on the air density. The calculation will be further explained in Section 5. The eigenvector, $\{q\}$, of the generalized coordinates contains the complex participation factor of each mode shape. Depending on the sign of the real part, the eigenvalue s expresses a positively or negatively damped oscillation:

$$\left\{ \overline{q}(t) \right\} = \mathrm{Re}\left(\{q\} e^{st} \right) = \mathrm{Re}\left(\{q\} e^{(\sigma + i\omega)t} \right). \tag{3}$$

Since a description of the aerodynamic force matrix using the complex reduced frequency is not always available, the aerodynamic terms are usually required to be purely harmonic motion, even when the vibrations of the entire system increase or decrease. The assumption of aerodynamic forces caused by harmonic motion is justified for the weakly damped situation close to the flutter stability limit. It presents an approximation for more strongly damped solutions. The contents of the bracket in Eq. (1) can be interpreted as the aeroelastic coefficient matrix $\left[F \right]$ for the solution vector $\{q\}$:

$$\left[F \left(s, k, M_\infty, \rho_\infty \right) \right] \{q\} = \{0\}. \tag{4}$$

At flutter onset however, only one solution branch usually becomes unstable at the critical flutter speed. For examination of the uncertainty of this flutter velocity with

regard to the uncertainties of the structural-dynamic model of the airplane, it makes sense to concentrate on this solution of the flutter equations and their variations. One should have a general overview of the flutter behavior by looking at the results of the established procedures. The p-k-method [10] and the g-method [6] iteratively solve the quadratic eigenvalue problem, whereby the starting value of the eigenvalue s and the flow velocity V_∞ are specified. Thereafter the critical solutions are pursued taking into account uncertainties defined in intervals. Reduction in the number of DoF. can often clarify the flutter mechanism.

Numerical continuation is a technique to generate successive points along a solution branch of a nonlinear equation system. Cardani and Mantegazza [5] developed an algorithm for the direct solution of the flutter equations using the continuation method to track various solutions dependent on free parameters. The solution vector $\{q\}$ of Eq.(4) is not determined in modulus and phase in the complex plane, which results in an infinite number of solutions. Only if one non-vanishing component is specified in modulus and phase, the system of equations has n-1 complex unknowns for $\{q\}$. The scaling together with an additional constraint for the relation of the imaginary part of the eigenvalue and the reduced frequency of (2) are introduced as additional constraint equations

$$\{y\} = \begin{Bmatrix} \left[F\left(s,k,M_\infty,\rho_\infty\right)\right]\{q\} \\ \{q\}^T\{q\} - 1 \\ \mathrm{Im}\left(s\right) - \dfrac{V_\infty}{c}k \end{Bmatrix} = \{0\}. \tag{5}$$

The complex system of equations contains $2\mathrm{n}+6$ unknowns

$$\{\hat{x}\}^T = \left\{\mathrm{Re}\left(q_1\right),\ldots,\mathrm{Re}\left(q_n\right),\mathrm{Im}\left(q_1\right),\ldots,\mathrm{Im}\left(q_n\right),\mathrm{Re}\left(s\right),\mathrm{Im}\left(s\right),k,V_\infty,M_\infty,\rho_\infty\right\}, \tag{6}$$

but only $2n+3$ equations. The determination of a unique solution requires the specification of three additional variables. With constant flight altitude and varying flight velocity, V_∞, the air density, ρ_∞, is known from the flight altitude. The relationship between speed of sound a_∞ and the true air speed V_∞ determines the Mach number M_∞. The increasing velocity can now be tracked by the continuation process, which provides converged solutions for each eigen pair after each continued step. Therefore, the expanded complex flutter equations in Eq.(5) are differentiated

with respect to the continued parameter V_∞ and transformed to an equivalent real system written as Jacobean coefficient matrix multiplied by the derivative of the solution vector $\{x\}$, which must be equal to the partial derivative of Eq.(5) with respect to V_∞:

$$\frac{d\{y\}}{d\{x\}} = \overbrace{\begin{bmatrix} \mathrm{Re}([F]) & -\mathrm{Im}([F]) & \mathrm{Re}\left(\frac{\partial[F]}{\partial s}\{q\}\right) & -\mathrm{Im}\left(\frac{\partial[F]}{\partial s}\{q\}\right) & \mathrm{Re}\left(\frac{\partial[F]}{\partial k}\{q\}\right) \\ \mathrm{Im}([F]) & \mathrm{Re}([F]) & \mathrm{Im}\left(\frac{\partial[F]}{\partial s}\{q\}\right) & \mathrm{Re}\left(\frac{\partial[F]}{\partial s}\{q\}\right) & \mathrm{Im}\left(\frac{\partial[F]}{\partial k}\{q\}\right) \\ \mathrm{Re}(\{q\})^T & -\mathrm{Im}(\{q\})^T & 0 & 0 & 0 \\ \mathrm{Im}(\{q\})^T & \mathrm{Re}(\{q\})^T & 0 & 0 & 0 \\ 0 & 0 & 0 & 1 & -\frac{V_\infty}{c} \end{bmatrix}}^{\frac{\partial\{y\}}{\partial\{x\}}} \overbrace{\begin{Bmatrix} \frac{d(\mathrm{Re}\{q\})}{dV_\infty} \\ \frac{d(\mathrm{Im}\{q\})}{dV_\infty} \\ \frac{d\sigma}{dV_\infty} \\ \frac{d\omega}{dV_\infty} \\ \frac{dk}{dV_\infty} \end{Bmatrix}}^{\frac{d\{x\}}{dV_\infty}} - \overbrace{\begin{Bmatrix} \mathrm{Re}\left(\frac{\partial[F]}{\partial V_\infty}\{q\}\right) \\ \mathrm{Im}\left(\frac{\partial[F]}{\partial V_\infty}\{q\}\right) \\ 0 \\ 0 \\ 0 \end{Bmatrix}}^{\frac{\partial(\{y\})}{\partial V_\infty}} = \{0\} \tag{7}$$

with

$$[F] = \left([M_{hh}]s^2 + [C_{hh}]s + [K_{hh}] - \frac{1}{2}\rho_\infty V_\infty^2 \left[Q_{hh}\left(M_\infty, k\right) \right] \right),$$

$$\frac{\partial[F]}{\partial V_\infty} = \left(\rho_\infty V_\infty [Q_{hh}] + \frac{1}{2}\frac{\rho_\infty V_\infty^2}{a_\infty}\frac{\partial[Q_{hh}]}{\partial M_\infty} \right),$$

$$\frac{\partial[F]}{\partial s} = \left(2s[M_{hh}] + [C_{hh}]\right),$$

$$\frac{\partial[F]}{\partial k} = -\frac{1}{2}\rho_\infty V_\infty^2 \frac{\partial[Q_{hh}]}{\partial k}$$

The MATLAB Toolbox MATCONT from Dhooge et al. [8] provides a numerical environment for the continuation method. The flutter equations are assumed as constant functions $f : \mathbb{R}^{n+1} \to \mathbb{R}^n$, for which the solution curve $f\left(\{x\}\right) = \{0\}$ should be calculated. For tracking purposes, it is necessary to have a starting solution $\{x_i\}$ and in addition the normalized tangent:

$$\{v_i\} = \left.\frac{d\{x\}}{dV_\infty}\right|_{V_{\infty,i}} \tag{8}$$

The calculation of the next point along the solution branch $\{x_{i+1}\}$ is composed of the following two steps: The prediction of the next point followed by the correction of that predicted point. The tangent extrapolates a new solution in direction of the continued parameter with an increment step size $h > 0$:

$$\left\{x^0\right\} = \left\{x_i\right\} + h\left\{v_i\right\}. \tag{9}$$

When the increment size h is selected small enough, the approximated solution $\left\{x^0\right\}$ is located close to the actual solution curve (see Fig. 1). In order to find the next point $\left\{x_{i+1}\right\}$ on the solution branch, the Newton algorithm is applied. Therefore, a further scalar auxiliary condition must be introduced. The hyperplane at the extrapolation $\left\{x^0\right\}$ must lie orthogonally to the tangential vector $\left\{v_i\right\}$:

$$\begin{Bmatrix} \left\{y\left(\left\{x\right\}\right)\right\} \\ \left(\left\{x\right\} - \left\{x^0\right\}\right)^T \left\{v_i\right\} \end{Bmatrix} = \left\{0\right\}. \tag{10}$$

Newton's iteration converges based on $\left\{x^0\right\}$ to a point $\left\{x_{i+1}\right\}$ on the solution curve, when the increment size h is small enough and the rank of the Jacobean matrix $\left[\frac{d\left\{y\right\}}{d\left\{x\right\}}\right]$ is equal to n.

The derivative in the direction of the continued parameter can be calculated using finite difference procedures for every continuation step, whereby the system of equations must be solved twice. Analytical calculated sensitivities may reduce computational costs.

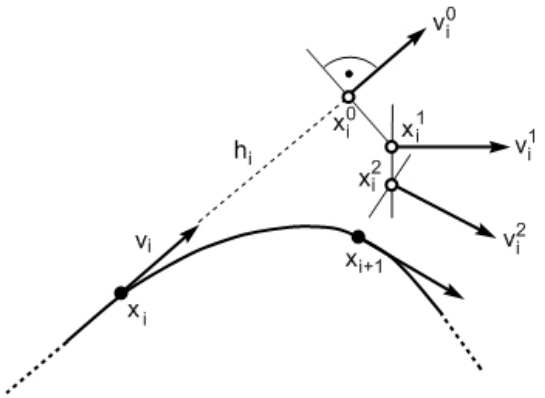

Figure 1, tracing of solution branch

This algorithm implemented in MATCONT uses an adaptive step-size control dependent on the curvature of the continued solution branch. Therefore, if the change of the resulting frequency and damping with respect to flight velocity is marginal, only very few steps are required to trace the velocity range. On the other

hand, if several solutions approach each other, which may result in rapidly changing or nearly merging damping or frequency curves, the continuation algorithm needs more sub-steps for the separation of the different solution branches.

4 Uncertainty propagation in modal analysis

In order to make a reliable statement on the flutter proneness of an aircraft for the intended range of operation, the interval ranges of all relevant parameters must be checked. For the uncertain variation range

$$\underline{u}_i \le u_i \le \overline{u}_i \tag{11}$$

statistical distributions can be assumed. For the aeroelastic stability analysis of airplane structures, the knowledge of a number of low-frequency eigen modes with eigen frequencies and modal masses is necessary. If an FE model is available, these data can be attained using arithmetical modal analysis. The equations of motion for a freely vibrating linear discrete system are

$$[M]\{\ddot{x}(t)\}+[C]\{\dot{x}(t)\}+[K]\{x(t)\}=\{0\}, \tag{12}$$

where $[M],[C],[K]\in\mathbb{R}^{N\times N}$ are the respective inertia, damping and stiffness matrices in N discrete physical DoF. and $\{x(t)\}\in\mathbb{R}^N$ contains the time-dependent deflections. The structural damping is usually assumed as a modal quantity. The dynamic characteristics of the undamped system are described with the solution of the linear eigenvalue problem

$$[K]\{\phi_j\}=\lambda_j[M]\{\phi_j\},\quad j=1\ldots m. \tag{13}$$

The eigenvectors are usually normalized to unit modal mass $\{\phi_j\}^T[M]\{\phi_j\}=1$. The nominal FE model should already render the vibration characteristics of the airplane. The mean and the variance of the uncertainties can then be approached as a parametric deviation of the first order of the nominal system:

$$\begin{aligned}[K]&=[K_0]+[\Delta K]=[K_0]+\sum_{i=1}^{r}u_i^{(k)}\left[K_i^{(k)}\right],\\ [M]&=[M_0]+[\Delta M]=[M_0]+\sum_{i=1}^{r}u_i^{(m)}\left[M_i^{(m)}\right]\end{aligned}. \tag{14}$$

The nominal inertia and stiffness matrices $[M_0]$ and $[K_0]$ may be the resulting mean value of a statistical distribution of the uncertain parameters.

$$\{u\}^T=\left\{u_1^{(k)}\ldots u_r^{(k)}\ u_1^{(m)}\ldots u_r^{(m)}\right\} \tag{15}$$

The deviations are shown as the sum of scalable macro-elements, where each can be composed of one single finite element, groups of elements or other substructures.

The partial system matrices $\left[K_r^{(k)}\right]$ and $\left[M_r^{(m)}\right]$ are scaled in such a manner, that the factors $u_r^{(k)}$ and $u_r^{(m)}$ are defined in the limits of the interval $[-1\ldots1]$ and may show a statistical distribution, e.g. standardised normal distribution, unified distribution etc.. The interval characteristics of the system matrices propagate through the eigenvalues and eigenvectors from Eq.(13). Even these can be expressed through mean centred nominal values with variance:

$$\begin{aligned}\lambda_j^I &= \lambda_j^C \pm \Delta\lambda_j \\ \left\{\phi_j^I\right\} &= \left\{\phi_j^C\right\} \pm \left\{\Delta\phi_j\right\}\end{aligned}. \tag{16}$$

Different methods can be applied to determine the deviation of the nominal value of the pairs of eigenvalues and eigenvectors. For non-probabilistic concepts, the interval modal analysis method is presented in the following.

4.1 Interval modal analysis method

In interval analysis, a pair of numbers representing the maximum and minimum values, in that the variable is expected to fall, replaces the value of the deterministic variable. Interval arithmetic rules are then used to perform mathematical operations with the interval numbers, which are also valid for each element in matrix operations.

The deterministic procedure of the finite-element eigenvalue analysis consists of the assembly of the parameter dependent system stiffness and mass matrices. Assuming independent interval system matrices, Deif [7] has shown that the bounds of the exact solution set of the interval eigenvalue problem are achieved for vertex matrix combination. Therefore, the solution phase introduces only conservatism through the artificial independence of the stiffness and mass matrix. Some algorithms have been developed that efficiently calculate the exact vertex solution of the interval eigen pairs. An overview is given by Moens et al. in [15]. In [16] Sim and Liu derived a formulation for interval modal analysis which is briefly reviewed In the following.

4.2 Mathematical background of interval algebra conventions

The definitions of the interval and interval operations is based on closed sets of real numbers denoted by $\mathbb{R}$. Its members are denoted by lower case letters. A subset of $\mathbb{R}$ of the form

$$x^I = [\underline{x}, \overline{x}] = \{t \mid \underline{x} \le t \le \overline{x}, \quad \underline{x}, \overline{x} \in \mathbb{R}\} \tag{17}$$

will be called a (closed) interval; $\underline{x}$ is the lower bound, and $\overline{x}$ is the upper bound.

Assuming that $I(\mathbb{R})$, $I(\mathbb{R}^n)$, and $I(\mathbb{R}^{n\times n})$ denote the sets of all closed real interval numbers, *n*-dimensional real interval vectors, and *n*×*n* real interval matrices, respectively. An *n*-dimensional real interval vector $\{x^I\} \in I(\mathbb{R}^n)$ can be written as

$$\{x^I\} = \{x_1^I, x_2^I, \ldots, x_n^I\}^{\mathrm{T}} \tag{18}$$

which can be usually written in the following form:

$$\{x^I\} = \left[\{x^c\} - \{\Delta x\}, \{x^c\} + \{\Delta x\}\right] \tag{19}$$

in which $\{x^c\}$ and $\{\Delta x\}$ denote the mean (or midpoint) value and the radius (or the maximum width) of $\{x^I\}$, respectively. It follows that

$$\begin{aligned} \{x^c\} &= \frac{\{\underline{x}\} + \{\overline{x}\}}{2} \\ \{\Delta x\} &= \frac{\{\overline{x}\} - \{\underline{x}\}}{2} \end{aligned} \tag{20}$$

Similar expressions exist for an *n*×*n* interval matrix

$$\begin{aligned} \left[A^I\right] &= \left[\left[\underline{A}\right], \left[\overline{A}\right]\right] \in I(\mathbb{R}^{n\times n}) \\ \left[A^I\right] &= \left[A^c\right] + \left[\Delta A\right] \end{aligned} \tag{21}$$

A^c and ΔA denote the mean matrix of A^I and the uncertainty (or the maximum width) is matrix A^I, respectively. It follows that

$$\begin{aligned} \left[A^c\right] &= \frac{\left[\overline{A}\right] + \left[\underline{A}\right]}{2} \\ a_{ij}^c &= \frac{\overline{a}_{ij} + \underline{a}_{ij}}{2} \\ \left[\Delta A\right] &= \frac{\left[\overline{A}\right] - \left[\underline{A}\right]}{2} \\ \Delta a_{ij} &= \frac{\overline{a}_{ij} - \underline{a}_{ij}}{2} \end{aligned} \tag{22}$$

Then following operations are valid:

$$x^I + y^I = [\underline{x}, \overline{x}] + [\underline{y}, \overline{y}] = [\underline{x} + \underline{y}, \overline{x} + \overline{y}] \tag{23}$$

$$x^I - y^I = [\underline{x}, \overline{x}] - [\underline{y}, \overline{y}] = [\underline{x} - \overline{y}, \overline{x} - \underline{y}] \tag{24}$$

$$x^I \times y^I = [\underline{x}, \overline{x}] \times [\underline{y}, \overline{y}] = \left[\min\left(\underline{x}\cdot\underline{y}, \underline{x}\cdot\overline{y}, \overline{x}\cdot\underline{y}, \overline{x}\cdot\overline{y}\right), \max\left(\underline{x}\cdot\underline{y}, \underline{x}\cdot\overline{y}, \overline{x}\cdot\underline{y}, \overline{x}\cdot\overline{y}\right)\right] \tag{25}$$

$$\frac{x^I}{y^I} = \frac{\left[\underline{x}, \overline{x}\right]}{\left[\underline{y}, \overline{y}\right]} = \left[\underline{x}, \overline{x}\right]\left[\frac{1}{\overline{y}}, \frac{1}{\underline{y}}\right] = \left[\frac{\underline{x}}{\overline{y}}, \frac{\overline{x}}{\underline{y}}\right] \tag{26}$$

Two sets $x^I = \left[\underline{x}, \overline{x}\right]$ and $y^I = \left[\underline{y}, \overline{y}\right]$ are equal if $\underline{x} = \underline{y}$ and $\overline{x} = \overline{y}$. An interval of zero width $x^I = \left[x, x\right]$ will be called as the point interval, and it is a regular real number. It is apparent that division is not defined if $0 \in \left[\underline{x}, \overline{x}\right]$ and that $c\left[\underline{x}, \overline{x}\right] = \left[c\underline{x}, c\overline{x}\right]$ for $c > 0$ and $c\left[\underline{x}, \overline{x}\right] = \left[c\overline{x}, c\underline{x}\right]$ for $c < 0$.

4.2.1 Interval eigen frequencies

If the stiffness and mass properties of a structure are affected by bounded uncertainties the intervals of the stiffness matrix and mass matrix can written as

$$\begin{aligned} &\left[\underline{K}\right] \le \left[K\right] \le \left[\overline{K}\right] \\ &\underline{k}_{ij} \le k_{ij} \le \overline{k}_{ij}, \quad i, j = 1, 2, \ldots, n \end{aligned} \tag{27}$$

$$\begin{aligned} &\left[\underline{M}\right] \le \left[M\right] \le \left[\overline{M}\right] \\ &\underline{m}_{ij} \le m_{ij} \le \overline{m}_{ij}, \quad i, j = 1, 2, \ldots, n \end{aligned} \tag{28}$$

With the use of the interval matrix notation, the above equations is rewritten as

$$\left[K\right] \in \left[K^I\right], \quad \left[K^I\right] = \left[\underline{K}, \overline{K}\right] = \left[\left[K^C\right] - \left[\Delta \mathrm{K}\right], \left[K^C\right] + \left[\Delta \mathrm{K}\right]\right] \tag{29}$$

$$\left[M\right] \in \left[M^I\right], \quad \left[M^I\right] = \left[\underline{M}, \overline{M}\right] = \left[\left[M^C\right] - \left[\Delta \mathrm{M}\right], \left[M^C\right] + \left[\Delta \mathrm{M}\right]\right] \tag{30}$$

in which $\left[K^I\right] = \left[\underline{K}, \overline{K}\right]$ is a positive-semidefinite symmetric interval matrix and $\left[M^I\right] = \left[\underline{M}, \overline{M}\right]$ is a positive-definite symmetric interval matrix. Then $\left[K^C\right]$ and $\left[M^C\right]$ are the centered interval stiffness and mass matrix, $\left[\Delta K\right]$ and $\left[\Delta M\right]$ are respectively the radius interval stiffness and mass matrix. The generalized interval eigenvalue problem can be expressed similar to the deterministic problem Eq.(13) by

$$\left[K^I\right]\left\{\phi_i^I\right\} = \lambda_i^I \left[M^I\right]\left\{\phi_i^I\right\} \tag{31}$$

Now, the centered eigenvalue problem for the *i*th eigenvector $\left\{\phi_i\right\}$ associated with the eigenvalue λ_i having interval parameter is considered:

$$\left[K^C\right]\left\{\phi_i\right\} = \lambda_i \left[M^C\right]\left\{\phi_i\right\} \tag{32}$$

The centered eigenvalues λ_i^C (natural frequencies) and the evaluative centered eigenvectors $\left\{\phi_i^C\right\}$ (normal modes) can now be obtained. To compute the lower and

the upper bounds on a particular eigenvalue λ_j^I, Deif's assumption is introduced from Ref. [7] assuming that the signs of the components of the associated eigenvector $\left\{\phi_i^C\right\}$ remain unchanged, when matrices $\left[K^I\right]=\left[\underline{K},\overline{K}\right]$ and $\left[M^I\right]=\left[\underline{M},\overline{M}\right]$ range over the interval. The diagonal sign matrix expressed by the sign of row elements of the *j*-th centered eigenvector is

$$\left[S_j\right]=diag\left(sgn\left(\phi_{1,j}^C\right),\ldots,sgn\left(\phi_{n,j}^C\right)\right). \tag{33}$$

In the sign matrix $\left[S_j\right]$ of the eigenvectors within the interval of the eigenvalues, the bounds found for the eigenvalues are exact. The lower bound $\underline{\lambda_i}$ and the upper bound $\overline{\lambda_i}$ satisfy the following two equations (see Qiu [18]):

$$\left(\left[K^C\right]-\left[S_j\right][\Delta K]\left[S_j\right]\right)\left\{\underline{\phi_j}\right\}=\underline{\lambda_j}\left(\left[M^C\right]+\left[S_j\right][\Delta M]\left[S_j\right]\right)\left\{\underline{\phi_j}\right\} \tag{34}$$

and

$$\left(\left[K^C\right]+\left[S_j\right][\Delta K]\left[S_j\right]\right)\left\{\overline{\phi_j}\right\}=\overline{\lambda_j}\left(\left[M^C\right]-\left[S_j\right][\Delta M]\left[S_j\right]\right)\left\{\overline{\phi_j}\right\} \tag{35}$$

where $\left\{\underline{\phi_j}\right\}$ and $\left\{\overline{\phi_j}\right\}$ are the eigenvectors corresponding to the upper-bound eigenvalue and lower-bound eigenvalue. In the general case of a system with relatively narrow system interval matrices, the interval eigenvalue problem is equivalent to the optimization problem to find the minimum or maximum of λ_j within the bounds.

By means of the above conclusion and the orthogonality demands of the modal parameters such as modal mass and modal stiffness, the modal interval parameters can be written as

$$\begin{aligned}\underline{k_j}&=\left\{\underline{\phi_j}\right\}^T\left(\left[K^C\right]-\left[S_j\right][\Delta\mathrm{K}]\left[S_j\right]\right)\left\{\underline{\phi_j}\right\}\\ \overline{k_j}&=\left\{\overline{\phi_j}\right\}^T\left(\left[K^C\right]+\left[S_j\right][\Delta\mathrm{K}]\left[S_j\right]\right)\left\{\overline{\phi_j}\right\}\end{aligned} \tag{36}$$

$$\begin{aligned}\underline{m_j}&=\left\{\overline{\phi_j}\right\}^T\left(\left[M^C\right]\text{-}\left[S_j\right][\Delta M]\left[S_j\right]\right)\left\{\overline{\phi_j}\right\}\\ \overline{m_j}&=\left\{\underline{\phi_j}\right\}^T\left(\left[M^C\right]+\left[S_j\right][\Delta M]\left[S_j\right]\right)\left\{\underline{\phi_j}\right\}\end{aligned} \tag{37}$$

From the relationship between the above modal parameters, the j-th modal interval eigenvalue is bounded by

$$\lambda_j^I = \left[\underline{\lambda}_j, \overline{\lambda}_j\right] = \left[\frac{\underline{k}_j}{\overline{m}_j}, \frac{\overline{k}_j}{\underline{m}_j}\right] = \left[\frac{\left\{\underline{\phi}_j\right\}^T \left[\underline{K}\right]\left\{\underline{\phi}_j\right\}}{\left\{\underline{\phi}_j\right\}^T \left[\overline{M}\right]\left\{\underline{\phi}_j\right\}}, \frac{\left\{\overline{\phi}_j\right\}^T \left[\overline{K}\right]\left\{\overline{\phi}_j\right\}}{\left\{\underline{\phi}_j\right\}^T \left[\underline{M}\right]\left\{\underline{\phi}_j\right\}}\right] \tag{38}$$

4.2.2 Interval mode shapes

In this section, the analysis of the "real" upper and lower bounds for mode shapes interval will be shown based on the first-order Taylor series expansion. When physical properties and geometric variables of structures are taken as structural parameters, the stiffness matrix and the mass matrix are functions of the structural parameters. The eigenvalue problem can be written in the form

$$\left[K\left(u_1^{(k)}, u_2^{(k)}, \ldots, u_r^{(k)}\right)\right]\left\{\phi_j\right\} = \lambda_j \left[M\left(u_1^{(m)}, u_2^{(m)}, \ldots, u_r^{(m)}\right)\right]\left\{\phi_j\right\} \tag{39}$$

with $\left\{\phi_j\right\}^T \left[M\right]\left\{\phi_j\right\} = 1$

If the eigenvalue problem subject to the upper- and lower-bound vectors is considered the structural parameter vector $\{u\}$ can be written as:

$$\left\{\underline{u}\right\} \le \left\{u\right\} \le \left\{\overline{u}\right\} \tag{40}$$

In terms of the interval matrix notation in interval mathematics or interval analysis, the inequality condition can be written as

$$\left\{u^I\right\} = \left[\left\{\underline{u}\right\}, \left\{\overline{u}\right\}\right] \tag{41}$$

By Taylor's series expansion, the eigenvector for the structural parameters $u_r = u_r^C + \Delta u_r, \quad r = 1, 2, \ldots, R$ is given by

$$\left\{\phi_j\left(u_1, u_2, \ldots, u_r\right)\right\} = \left\{\phi_j\left(u_1^C, u_2^C, \ldots, u_r^C\right)\right\} + \sum_{i=1}^{r} \frac{\partial\left\{\phi_j\left(u_1^C, u_2^C, \ldots, u_r^C\right)\right\}}{\partial u_i}\left(u_i - u_i^C\right) \tag{42}$$

It is understood that in the summation, the partial derivative is taken and then evaluated at the centered value, which can be obtained by the first-order perturbation theory as follows:

$$\frac{\partial\left\{\phi_j\right\}}{\partial u_i} = \sum_{k=1}^{r} c_{jk}\left\{\phi_j\right\}, \tag{43}$$

where

$$c_{jk} = \frac{1}{\lambda_{ic} - \lambda_{sc}}\left\{\phi_k^C\right\}^T \frac{\partial\left[K\left(u^C\right)\right]}{\partial u_i}\left\{\phi_j^C\right\} - \lambda_j^C \left\{\phi_k^C\right\}^T \frac{\partial\left[M\left(u^C\right)\right]}{\partial u_i}\left\{\phi_j^C\right\} \quad for\ (k \neq j)$$

and

$$c_{jj} = -\frac{1}{2}\left\{\phi_k^C\right\}^T \frac{\partial\left[M\left(u^C\right)\right]}{\partial u_i}\left\{\phi_j^C\right\} \quad for\ (k = j)$$

The objective now is to find the lower-bound eigenvector and the upper-bound eigenvector of the eigenvector for all possible structural parameters, which becomes the following extreme value problem:

$$\left\{\phi_j^{(ext)}\right\} = extremum\left(\left\{\phi_j^C\right\} + \frac{\partial\left\{\phi_j\left(u^C\right)\right\}}{\partial u_i}\Delta u_i\right) \tag{44}$$

The lower- and upper bounds of the eigenvector can then be obtained from

$$\begin{aligned}\left\{\underline{\phi}_j\right\} &= \left\{\phi_j^C\right\} - \sum_{i=1}^{r}\left|\frac{\partial\left\{\phi_j^C\right\}}{\partial u_i}\right|\Delta u_i \\ \left\{\overline{\phi}_j\right\} &= \left\{\phi_j^C\right\} + \sum_{i=1}^{r}\left|\frac{\partial\left\{\phi_j^C\right\}}{\partial u_i}\right|\Delta u_i\end{aligned} \tag{45}$$

4.2.3 Modal transformation of interval structural dynamics system

While this interval modal analysis has been applied successfully to small problems, it has not been found practical for large simulations because the results are in many cases too conservative, i.e. it predicts the greatest possible uncertainty in the output. On the other hand, the modal transformation from physical to modal DoF. (see flutter equations Eq.(1)) reduces the problem size significantly to the modal degrees of freedom. As for flutter analysis, only the lower frequency band must be considered, which includes usually up to 10^2 modal DoF., in spite of $10^4 - 10^7$ in physical space of an industrial FE-model. The fundamental question is the procedure to build an expanded modal basis $[B]$, that gives good predictions for all desired ranges in the modal space dependent on the uncertain parameter vector $\left\{u^I\right\}$. In [2] Balmes considered a few classical solutions:

- The basis of nominal modes should include more mode shapes than needed for the chosen frequency range under consideration: $[B] = \left[\Phi_{1..m}\left\{u^c\right\}\right]$.
- The enrichment of this basis by inclusion of mode shape sensitivities with respect to uncertain parameters, which are calculated by the method of Fox

and Kapoor [9], can significantly extend the range of validity:

$$[B] = \left[\left[\Phi_{1\ldots m} \left\{ u^c \right\} \right] \quad \frac{\partial \left[\Phi_{1\ldots m} \left\{ u^c \right\} \right]}{\partial \{u\}} \right].$$

- For multi-model basis mode shapes predictions are exact for the retained values at the lower and upper bounds of the parameter space and fairly good between those points:

$$[B] = \left[\left[\Phi_{1\ldots m} \left\{ \underline{u} \right\} \right] \quad \left[\Phi_{1\ldots m} \left\{ \overline{u} \right\} \right] \right].$$

Hence the eigenvalue problem from Eq.(13) can be reanalyzed in the modal subspace:

$$\left([B]^T \left[K^C \right] [B] \right) \left\{ \psi_j^C \right\} = \lambda_j^C \left([B]^T \left[M^C \right] [B] \right) \left\{ \psi_j^C \right\} \tag{46}$$

Restitution of responses on all physical DoF. is then simply given by

$$\left\{ \phi_j \right\} = [B] \left\{ \psi_j \right\}. \tag{47}$$

In practice, ortho-normalization of the expanded basis must be performed before appending the enrichment. The algorithm of Balmes [3] using singular value decomposition calculates the reduced not rank-deficient basis. If this subspace transformation is introduced in Eq.(34) and (35), approximate solutions of the lower and upper bounds can be calculated independent of the uncertain parameters $\{u\}$:

$$\begin{aligned} &\left([B]^T [K^C] [B] - [S_j] [B]^T [\Delta K] [B] [S_j] \right) \left\{ \underline{\psi}_j \right\} \\ &\qquad = \underline{\lambda}_j \left([B]^T [M^C] [B] + [S_j] [B]^T [\Delta M] [B] [S_j] \right) \left\{ \underline{\psi}_j \right\} \end{aligned} \tag{48}$$

$$\begin{aligned} &\left([B]^T [K^C] [B] + [S_j] [B]^T [\Delta K] [B] [S_j] \right) \left\{ \overline{\psi}_j \right\} \\ &\qquad = \overline{\lambda}_j \left([B]^T [M^C] [B] - [S_j] [B]^T [\Delta M] [B] [S_j] \right) \left\{ \overline{\psi}_j \right\} \end{aligned} \tag{49}$$

with

$$[S_j] = diag \left(sgn \left(\psi_{j,i}^C \right), \ldots, sgn \left(\psi_{j,m}^C \right) \right) \tag{50}$$

For each mode shape under consideration, the reanalysis of frequency and shape intervals for both combinations can thus be very fast using the following relationship:

$$\begin{aligned} \left(\omega_j^I \right)^2 &= \left[\left(\lambda_j^C - \Delta\lambda_j \right), \left(\lambda_j^C + \Delta\lambda_j \right) \right], \\ \left\{ \phi_j^I \right\} &= \left[[B] \left\{ \psi_j^C - \Delta\psi_j \right\}, [B] \left\{ \psi_j^C + \Delta\psi_j \right\} \right] \end{aligned} \tag{51}$$

5 Uncertainty propagation in flutter analysis

In the flutter equations Eq.(1), the unsteady aerodynamic forces are induced by harmonic oscillation of the aircraft structure. For the calculation, an aerodynamic theory must be applied, that provides the aerodynamic forces for specified reduced frequencies k and Mach numbers M_∞. As a widely used unsteady aerodynamic theory, the well-known Doublet Lattice Method, DLM [1], has proven to be reliable and has become the aeroelastic standard procedure for the subsonic compressible flight range used by the industry for many years. One of the main advantages compared with the modern CFD-methods is the independency of the aerodynamic influence coefficient matrix with respect to the structural deflection. The aerodynamic database for a fixed geometry and several reduced frequencies and Mach numbers can be calculated in advance. During the flutter analysis, the modal aerodynamic loads are generated by pre- and post-multiplication of the deflections of the mode shapes. The pressure difference $\{c_p\}$ between the upper and lower side of each elementary lifting surface element can be linked to the downwash via an aerodynamic influence coefficient matrix $[AIC]$:

$$\{c_{p,i}\} = [AIC(M_\infty, k)]\left(\frac{\partial\{\phi_i\}}{\partial x} + \frac{i\omega}{V}\{\phi_i\}\right). \tag{52}$$

The downwash of every aerodynamic element is linked to the motion of the lifting surface. Here, the first term corresponds to in-phase local angle of attack and the second term to out of phase component, which results from the surface velocity perpendicular to the mean flow velocity. The transformation of the spatially distributed deflection into the local system of the lifting surfaces can be conducted by interpolation. The linearized spatial transformation can be summarized in a constant matrix, $[T]$, and its spatial derivative in flow direction, $\left[\frac{\partial T}{\partial x}\right]$, that is pre-multiplied to the interval modal matrix from Eq.(51):

$$\left[w^I\right] = \left(\frac{\partial[T]}{\partial x} + i\frac{k}{c}[T]\right)\left[\Phi^I\right]. \tag{53}$$

The modal aerodynamic force matrix is then also expressed as an interval matrix:

$$\left[Q_{hh}^{C} \pm \Delta Q_{hh}\right] = \left[\Phi^{C} \pm \Delta\Phi\right]^{T} \left([T]^{T} [A] \left[AIC\left(M_{\infty}, k\right)\right] \left(\frac{\partial [T]}{\partial x} + i \frac{k}{c} [T] \right) \right) \left[\Phi^{C} \pm \Delta\Phi\right]. \quad (54)$$

Here the matrix $[A] = \left[diag\left\{A_1, A_2, \ldots, A_m\right\}\right]$ includes the surface areas of the aerodynamic elements for integration of the pressures to aerodynamic forces. The centered and radius modal aerodynamic loads matrices can be written as:

$$\begin{aligned} \left[Q_{hh}^{C}\right] &= \left[\Phi^{C}\right]^{T} \left[GAIC\left(M_{\infty}, k\right)\right] \left[\Phi^{C}\right]. \quad (55) \\ \left[\Delta Q_{hh}\right] &= \left[\Phi^{C}\right]^{T} \left[GAIC\left(M_{\infty}, k\right)\right] \left[\Delta\Phi\right] \\ &+ \left[\Phi^{C}\right]^{T} \left[GAIC\left(M_{\infty}, k\right)\right] \left[\Delta\Phi\right] \\ &+ \left[\Delta\Phi\right]^{T} \left[GAIC\left(M_{\infty}, k\right)\right] \left[\Delta\Phi\right] \\ \left[GAIC\left(M_{\infty}, k\right)\right] &= \left([T]^{T} [A] \left[AIC\left(M_{\infty}, k\right)\right] \left(\frac{\partial [T]}{\partial x} + i \frac{k}{c} [T] \right) \right) \end{aligned}$$

5.1 Interval flutter analysis method

The flutter equation Eq.(4) can be reformulated for fixed density and velocity but with intervals for the structural mass, damping and stiffness matrices resulting from modal analysis and :

$$\left(\left[M_{hh}^{C} \pm \Delta M_{hh}\right] s^2 + \left[C_{hh}^{C} \pm \Delta C_{hh}\right] s + \left[K_{hh}^{C} \pm \Delta K_{hh}\right] - \frac{1}{2} \rho_{\infty} V_{\infty}^{2} \left[Q_{hh}^{C} \pm \Delta Q_{hh}\right] \right) \{q\} = \{0\}. \quad (56)$$

In accordance to Eq. (7) the differential of the equivalent real flutter equations can now be written with respect to the combination of the uncertain parameter set:

$$\frac{d\{y\}}{d\{x\}} = \overbrace{\begin{bmatrix} \mathrm{Re}([F]) & -\mathrm{Im}([F]) & \mathrm{Re}\left(\frac{\partial [F]}{\partial s}\{q\}\right) & -\mathrm{Im}\left(\frac{\partial [F]}{\partial s}\{q\}\right) & \mathrm{Re}\left(\frac{\partial [F]}{\partial k}\{q\}\right) \\ \mathrm{Im}([F]) & \mathrm{Re}([F]) & \mathrm{Im}\left(\frac{\partial [F]}{\partial s}\{q\}\right) & \mathrm{Re}\left(\frac{\partial [F]}{\partial s}\{q\}\right) & \mathrm{Im}\left(\frac{\partial [F]}{\partial k}\{q\}\right) \\ \mathrm{Re}(\{q\})^{T} & -\mathrm{Im}(\{q\})^{T} & 0 & 0 & 0 \\ \mathrm{Im}(\{q\})^{T} & \mathrm{Re}(\{q\})^{T} & 0 & 0 & 0 \\ 0 & 0 & 0 & 1 & -\frac{V_{\infty}}{c} \end{bmatrix}}^{\frac{\partial\{y\}}{\partial\{x\}}} \overbrace{\begin{Bmatrix} \frac{d(\mathrm{Re}\{q\})}{du} \\ \frac{d(\mathrm{Im}\{q\})}{du} \\ \frac{d\sigma}{du} \\ \frac{d\omega}{du} \\ \frac{dk}{du} \end{Bmatrix}}^{\frac{d\{x\}}{du}} - \overbrace{\begin{Bmatrix} \mathrm{Re}\left(\frac{\partial [F]}{\partial u}\{q\}\right) \\ \mathrm{Im}\left(\frac{\partial [F]}{\partial u}\{q\}\right) \\ 0 \\ 0 \\ 0 \end{Bmatrix}}^{\frac{\partial\{y\}}{\partial u}} = \{0\} \quad (57)$$

with

$$\frac{\partial [F]}{\partial u_i} = \frac{[\Delta F]}{\Delta u_i} = \pm \left[\Delta M_{hh}\right] s^2 \pm \left[\Delta C_{hh}\right] s \pm \left[\Delta K_{hh}\right] \pm \frac{1}{2} \rho_{\infty} V_{\infty}^{2} \left[\Delta Q_{hh}\left(M_{\infty}, k\right)\right] \quad (58)$$

The perturbed non-linear flutter equations at the upper and lower bounds are solved by applying Newton's method available from the toolbox of the continuation method:

$$\begin{aligned}\{\underline{x}_{i+1}\} &= \{\underline{x}_i\} - \left[\left.\frac{\partial\{y\}}{\partial\{x\}}\right|_{\{\underline{x}_i\}}\right]^{-1} \frac{\partial\{y\}}{\partial u_i}\Delta u_i \\ \{\overline{x}_{i+1}\} &= \{\overline{x}_i\} + \left[\left.\frac{\partial\{y\}}{\partial\{x\}}\right|_{\{\overline{x}_i\}}\right]^{-1} \frac{\partial\{y\}}{\partial u_i}\Delta u_i\end{aligned} \tag{59}$$

after each converged flight velocity continuation steps, the procedure must be repeated for all combinations of identified critical parameter sets to find the minimum and maximum of the eigenvalue of the aeroelastic system. As the nominal solution $\{x^0\}$ is already known it can be used as adequate starting vector for the iterations. The solution generally converges in very few steps, so that the uncertainty bounds in frequency and damping can be calculated during the main flutter analysis process. The intervals of critical damping and frequency as part of the interval solution vector $\left[\{\underline{x}\},\{\overline{x}\}\right]$ can then be extracted from lower and upper bounds using an Boolean matrix for each parameter:

$$\begin{aligned}\Delta\sigma_i &= \begin{bmatrix}0 & \cdots & 0 & 1 & 0\end{bmatrix}\left[\frac{\partial\{y\}}{\partial\{x\}}\right]^{-1} \frac{\partial\{y\}}{\partial u_i}\Delta u_i \\ \Delta\omega_i &= \begin{bmatrix}0 & \cdots & 0 & 0 & 1\end{bmatrix}\left[\frac{\partial\{y\}}{\partial\{x\}}\right]^{-1} \frac{\partial\{y\}}{\partial u_i}\Delta u_i\end{aligned} \tag{60}$$

This procedure is repeated after each solution step of the nominal solution $\{x^0\}$ during the application of the continuation process introduced in chapter 3. If the perturbation of the four uncertain system matrices in the flutter equations Eq.(58) is uncorrelated all combination of system matrix perturbation at lower and upper bounds must be evaluated, which results $2^4 = 16$ sensitivity calculations.

$$\left[U\right] = \begin{bmatrix} -1 & -1 & -1 & -1 \\ -1 & -1 & -1 & 1 \\ -1 & -1 & 1 & -1 \\ -1 & -1 & 1 & 1 \\ -1 & 1 & -1 & -1 \\ -1 & 1 & -1 & 1 \\ -1 & 1 & 1 & -1 \\ -1 & 1 & 1 & 1 \\ 1 & -1 & -1 & -1 \\ 1 & -1 & -1 & 1 \\ 1 & -1 & 1 & -1 \\ 1 & -1 & 1 & 1 \\ 1 & 1 & -1 & -1 \\ 1 & 1 & -1 & 1 \\ 1 & 1 & 1 & -1 \\ 1 & 1 & 1 & 1 \end{bmatrix} \tag{61}$$

Structural damping is often neglected, so that the number of evaluations reduces to $2^3 = 8$ combinations.

The search for minimum and maximum damping and frequency of the aeroelastic system will determine the uncertain response intervals, which can be plotted as error bars or shaded areas in the flutter diagrams. The workflow for the solutions of the flutter equations by application of the continuation method including uncertainty analysis is presented in Figure 2.

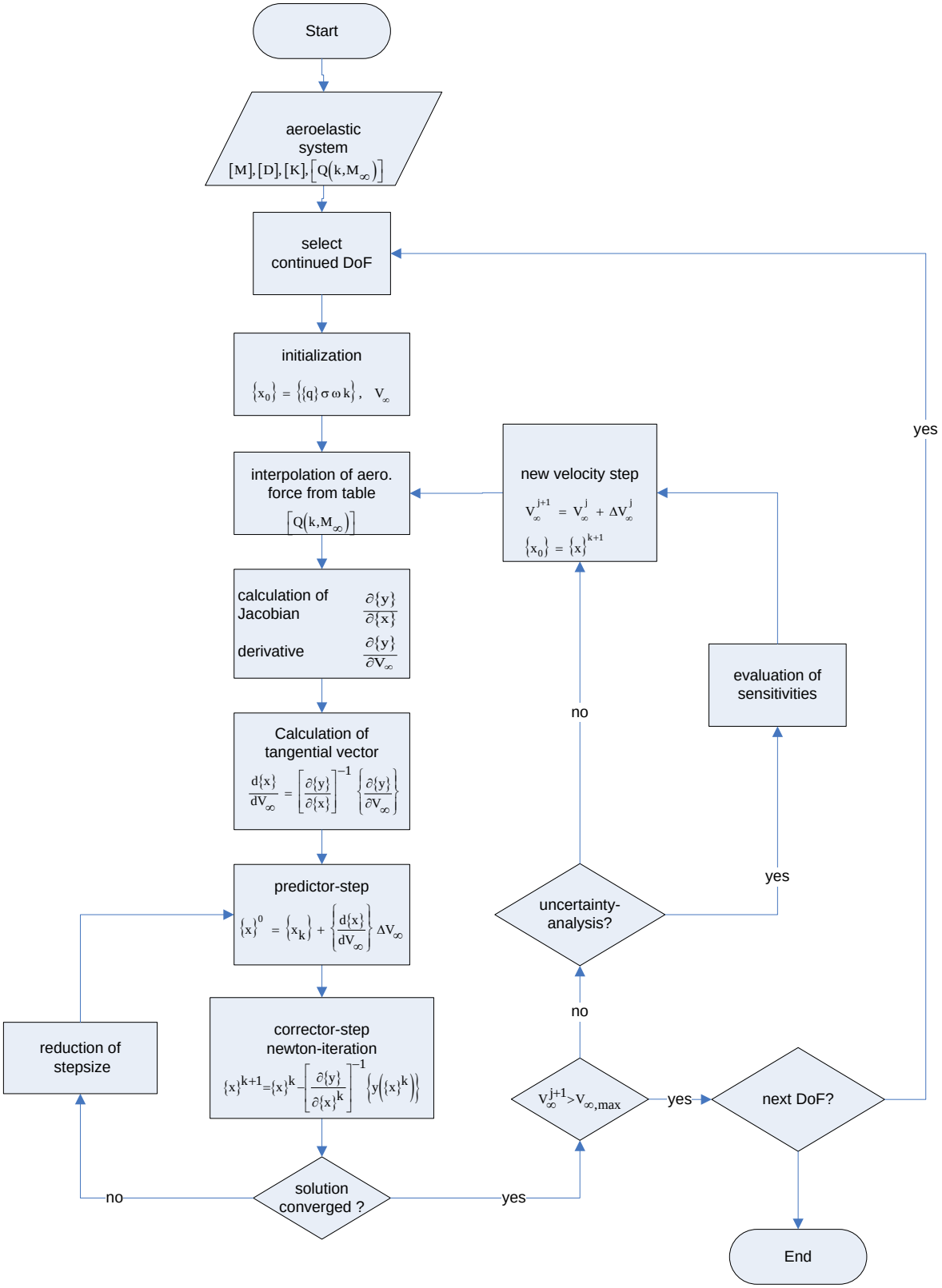

Figure 2, workflow of continuation method including uncertainty analysis

6 Numerical example

The presented flutter analysis method is applied to the example aircraft I23, which is a single-engine, four-seat low-wing monoplane with typical manual driven control surfaces and three-wheel landing gear. The airframe structure is made mainly of composite materials. The aircraft has been manufactured in compliance with FAR-23 regulations is designed to perform executive flights in normal and difficult weather conditions and to train the pilots for IFR flights, take-off and landing and ILS landing.

For this aircraft an Finite Element Model for the commercial software MSC/NASTRAN is available which includes modelling of the full mechanical control system from pilot controls to the control surfaces (see Figure 3). As with manual controlled aircraft the control surfaces may participate in flutter instabilities, it is mandatory for reliable flutter stability forecast to implement a correct idealisation of all control devices. Modal analysis is applied to the FE-model to calculate the mode shapes of the first 40 eigen frequencies. The eigen frequencies are summarized in Table 2. Plots of all mode shapes can be found in the Appendix A. It can be observed that all mode shape include contribution of control surface deflections. The mode shape deflections of the FE-model are interpolated to the aerodynamic mesh of the DLM. The applied volume spline method was modified in [19] for application of reduced mode shape data. In ground vibration tests the acceleration of only a limited number of physical DoF can be measured. Usually 50-100 sensor are fitted to the structure. In Figure 4 the deflection transfer for the fundamental bending is shown and as an example of a control mode in Figure 5.

The software including all modules is implemented in MATLAB as aeroelastic toolbox AETB. Only the applied DLM for calculation of the aerodynamic influent coefficients is a FORTRAN implementation, which is used as mex-function in MATLAB and is based of the implementation of reference [2], which utilizes the quartic approximation of the kernel function.

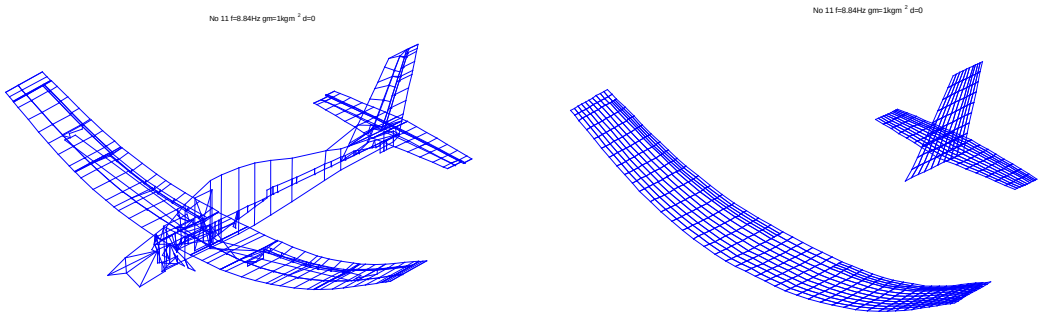

Figure 3, airframe mode shape of FE model and DLM model

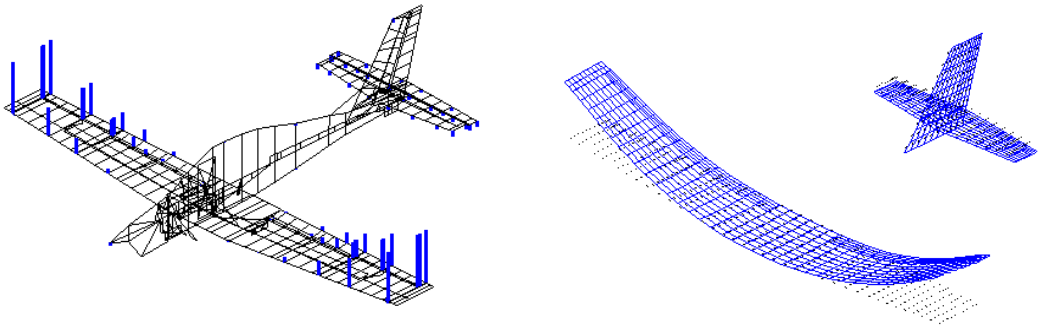

Figure 4, Interpolation of GVT results to DLM mesh, airframe mode

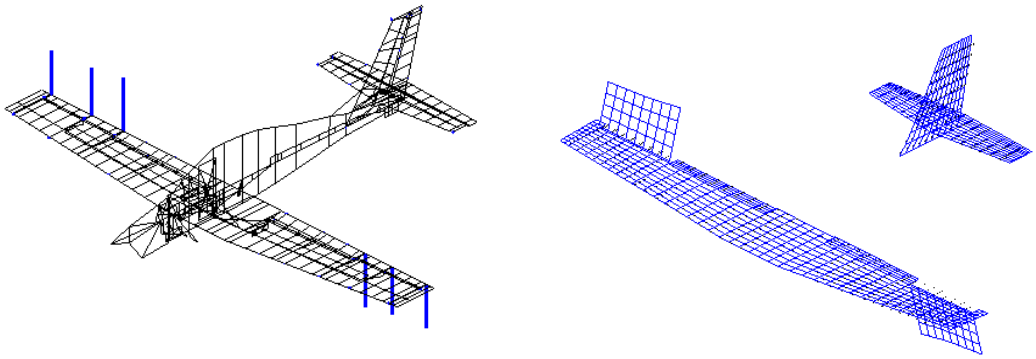

Figure 5, Interpolation of GVT results to DLM mesh, control mode

6.1 I23-Flutter results of nominal FEM

For evaluation of the presented continuation method several flutter calculations were performed in comparison to the flutter results of the commercial aeroelastic software ZAERO. The damping and frequency of the ZAERO results can be found in Figure 6 for sea level up to maximum speed of 600km/h. In Figure 7 the comparable results of the continuation method are plotted. In addition a third flutter analysis was based on the FE mode shapes, but for the interpolation to the aerodynamic mesh only the sensor degrees of freedom measured during GVT were used. The damping and frequency curves can be found in Figure 8. In Table 1 the critical flutter speeds of all flutter results are compared. It can be seen that the speeds for the modes with rapid damping decrease are in good agreement. The modes with smooth decrease show much more deviation. In Figure 13 animations of the complex flutter mode shapes are plotted.

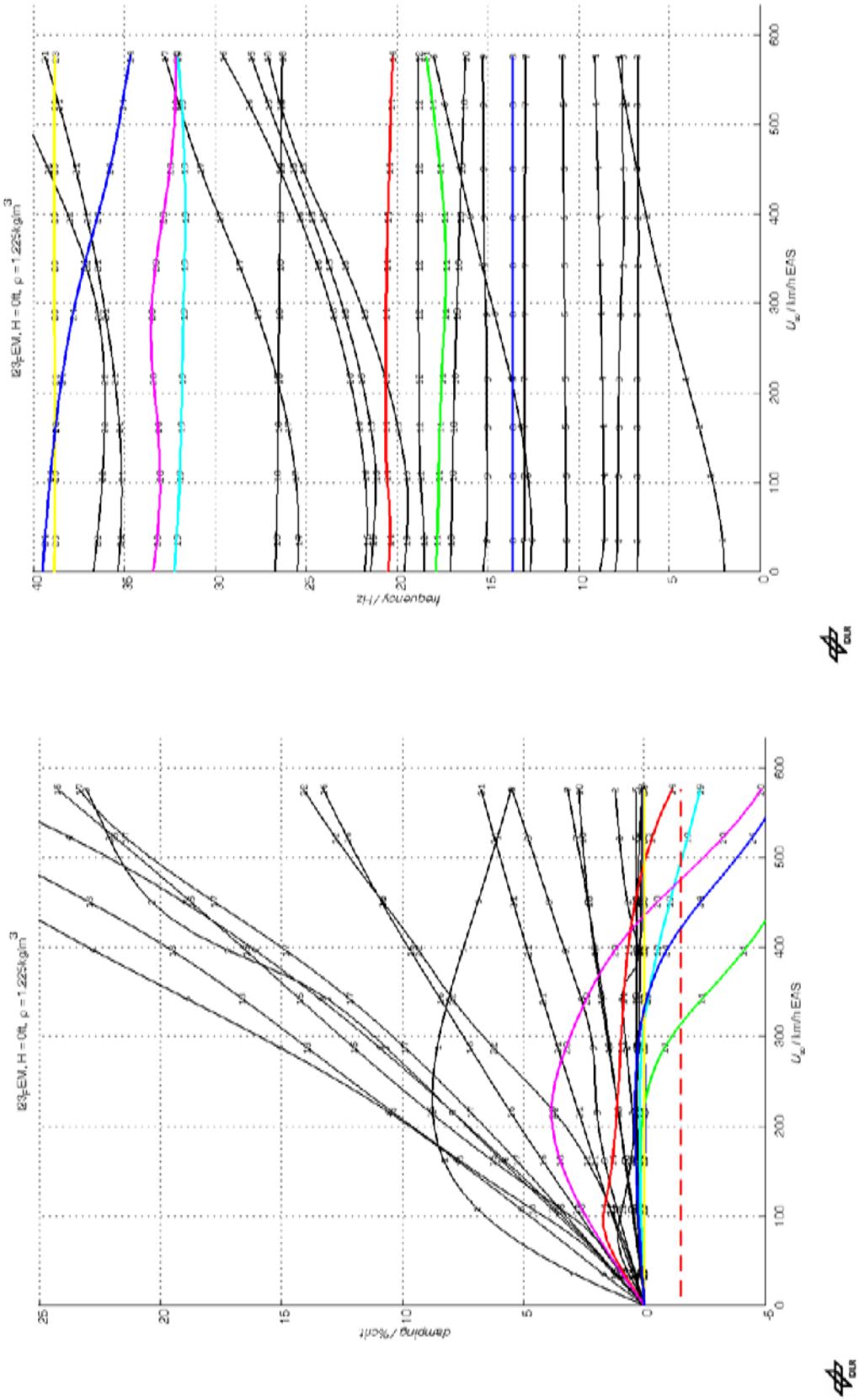

Figure 6, V-f and V-g diagrams, ZAERO analysis

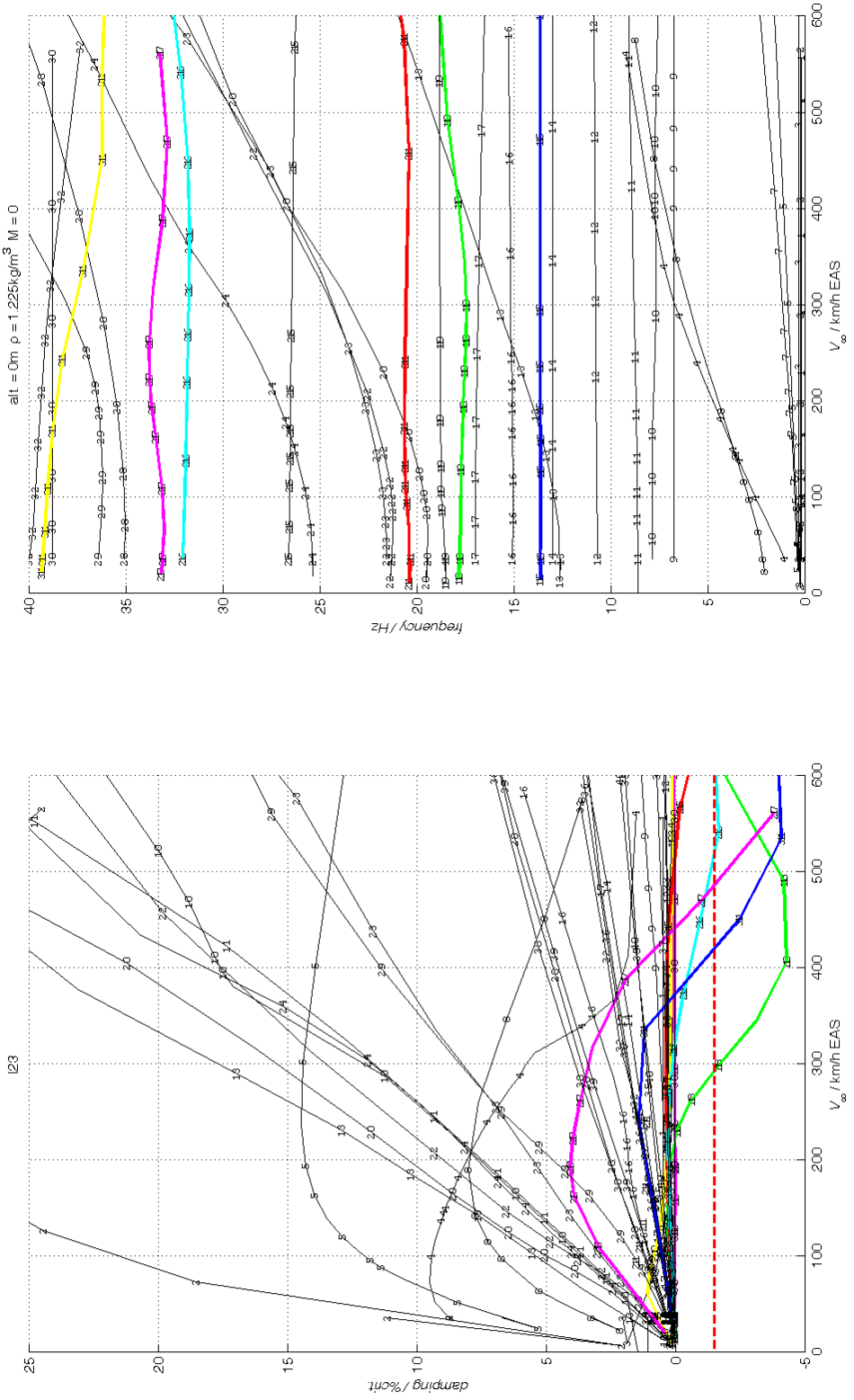

Figure 7, V-f and V-g diagrams, continuation method with FEM-mode shapes

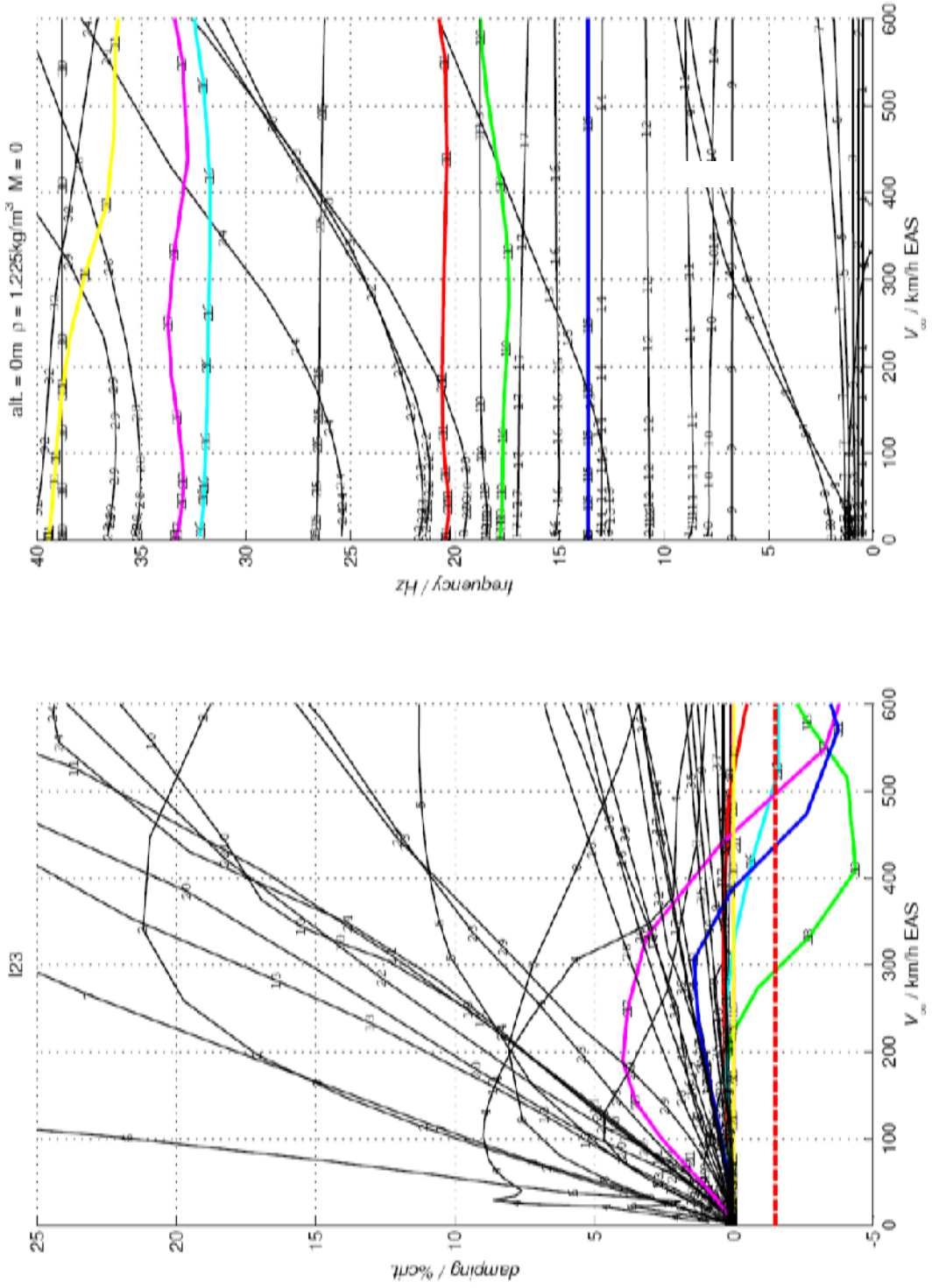

Figure 8, V-f and V-g diagrams, continuation method with incomplete FEM-mode shapes (GVT sensor dof)

Table 1, comparison of flutter results GVT – ZAERO – FLACONT- FLACONT with incomplete mode shapes

Flutter mode	FEM+ZAERO		FEM+FLACONT FEM DoF		FEM+FLACONT GVT DoF	
	V	f	V	f	V	f
	km/h	Hz	km/h	Hz	km/h	Hz
A	223.4	17.5	222.0	17.5	223.2	17.5
B	317.2	31.7	321.8	31.7	323.5	31.7
C	331.9	37.3	372.5	36.9	388.4	36.6
D	493.2	20.4	412.5	20.4	425.9	20.4
E	435.2	32.5	441.7	32.9	452.89	32.8

A fuselage torsion / rudder rotation with horizontal tailplane yawing

B antisymmetrical wing bending with flaps rotation

C antisymmetrical wing torsion with aileron+flaps rotation

D vertical tailplane bending with rudder rotation

E symmetrical wing torsion with flaps rotation

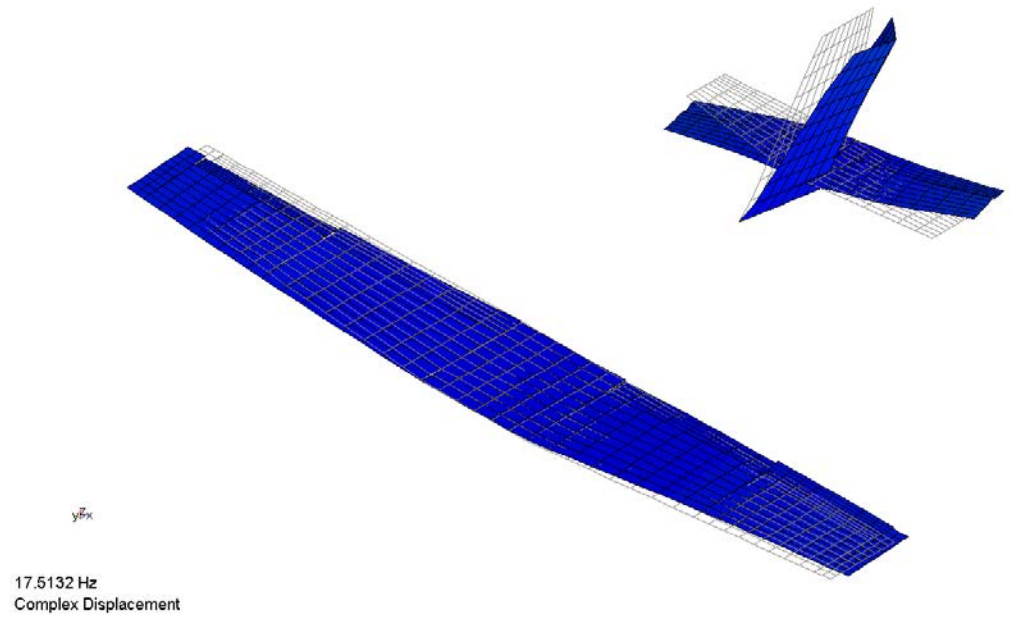

Figure 9, flutter mode A, fuselage torsion / rudder rotation with horizontal tailplane yawing, 222.0 km/h EAS, 17.5Hz

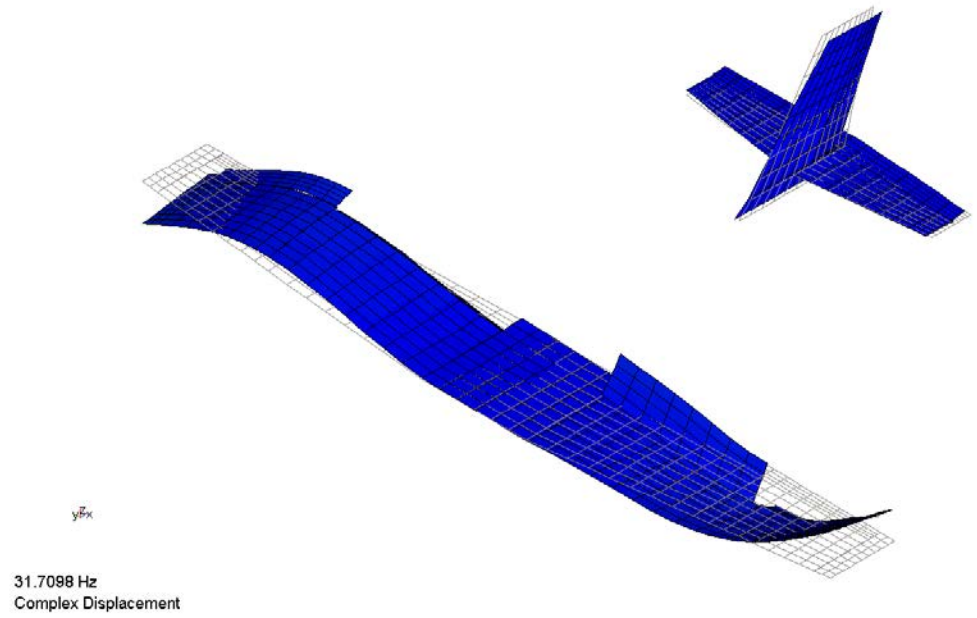

Figure 10, flutter mode B, antisymmetrical wing bending with flaps rotation, 321.8km/h EAS, 31.7Hz

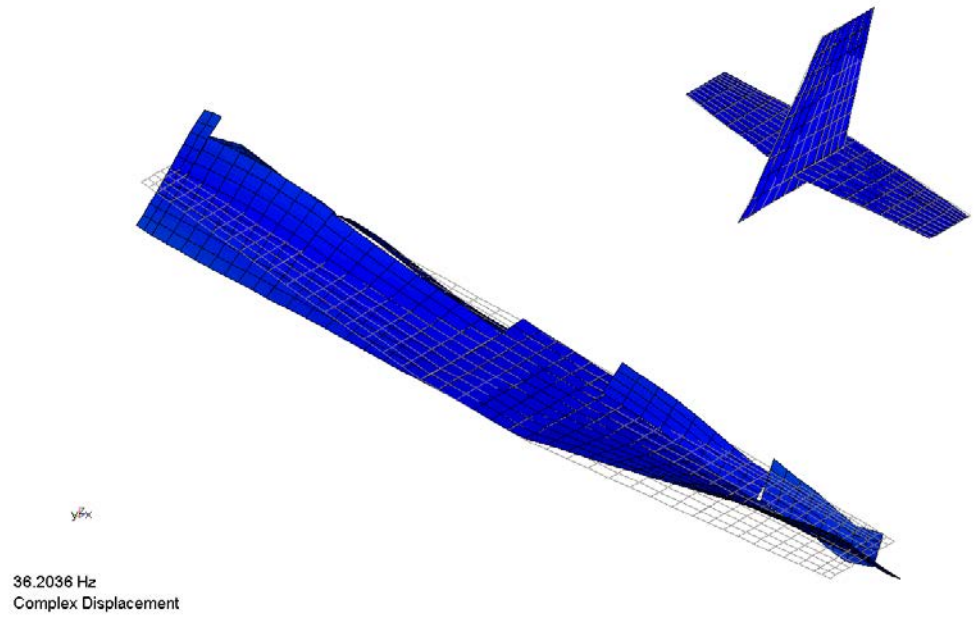

Figure 11, flutter mode C, antisymmetrical wing torsion with aileron+flaps rotation, 372.5km/h EAS, 36.9Hz

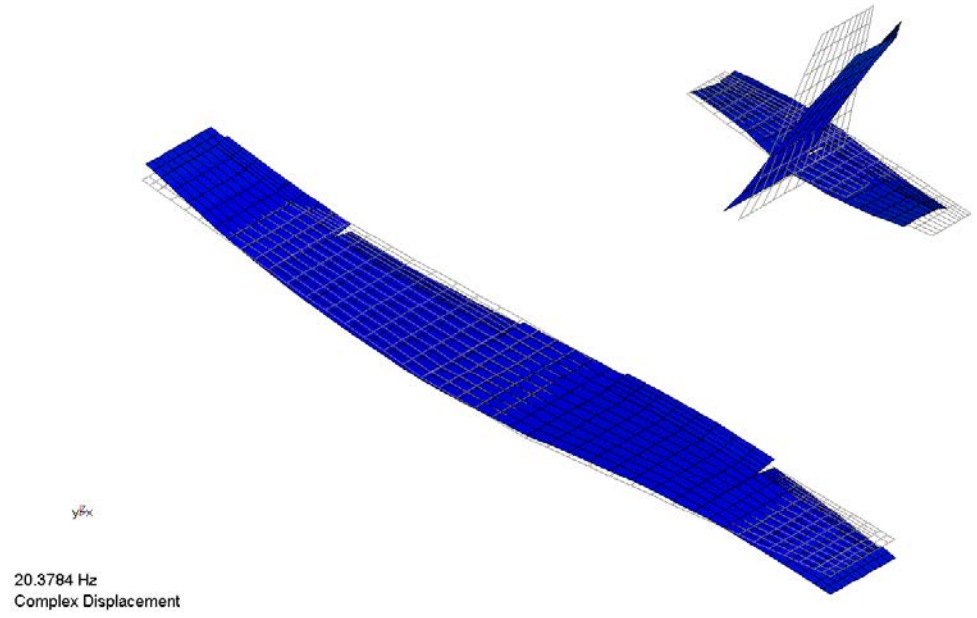

Figure 12, flutter mode D, vertical tailplane bending with rudder rotation, 412.5km/h EAS, 20.4Hz

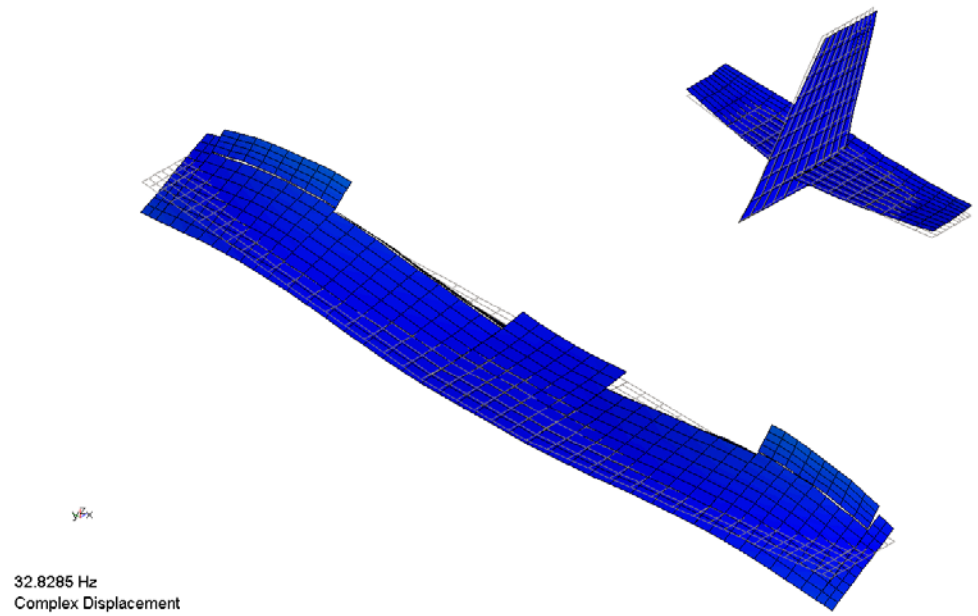

Figure 13, flutter modes E, symmetrical wing torsion with flaps rotation, 441.7km/h EAS, 32.9Hz

6.2 I23 Flutter results with varying air density

Aeroelastic stability of an aircraft must be granted for the whole flight envelope. One varying physical parameter is the air density which is a linear factor to the unsteady aerodynamic forces in the flutter equations. Usually flutter analyses are performed for several flight altitudes to cover the effects of the density. As this parameter can also be bounded by an interval, the continuation method with interval search can be applied. In Figure 14 the resulting ranges of dampings and frequencies are plotted for the varyibg altitude between 0m MSL and 5000m MSL. It can be observed that dampings are considerably affected by the density.

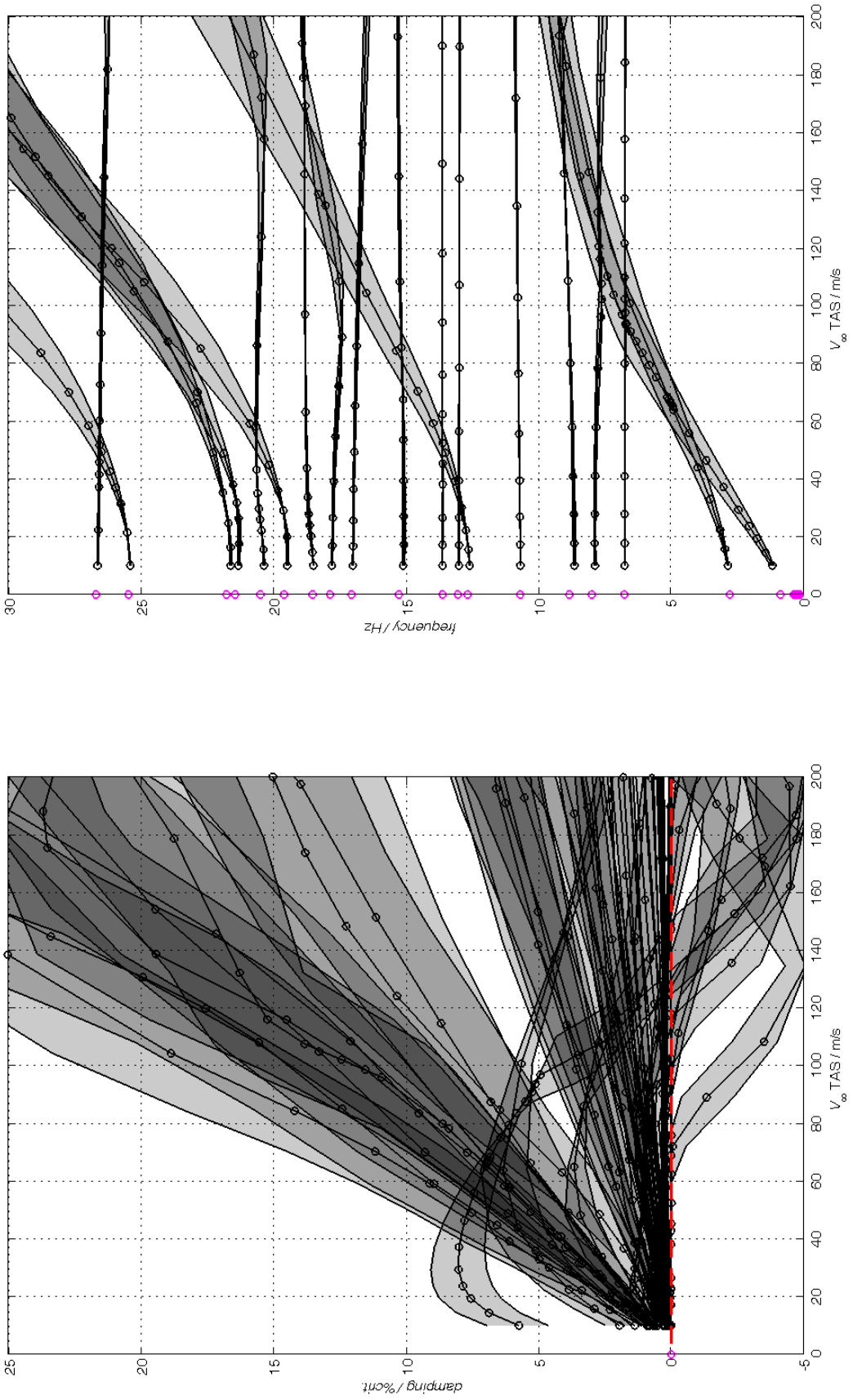

Figure 14, V-f and V-g diagrams, continuation method with varying flight altitude 0m<h<5000m

6.3 I23 Flutter results including control surface mass variations

As already mentioned the control surface properties especially in mass have strong influence in the stability behaviour. Depending on the manufacturing process the mass of control surfaces can vary in production. Here it is assumed that the mass tolerances of control surface masses is +/-20%. Therefore, the identified flutter cases with lowest critical flutter speed and contribution of rudder and aileron are under investigation. The interval modal analysis is applied to the I23 FE model to find the ranges of eigen frequencies and mode shapes. In Table 2 the eigen frequencies of nominal model and for the lower and upper control surface mass bound are summarized together with the procentile deviations, which is 8.4% in maximum.

The intervals of the dampings and frequencies of unstable couplings with the rudder deflection starting at 12.67Hz are shown in Figure 15. These are two bending modes of the vertical tailplane at 17.58Hz and 20.5Hz.

In Figure 16 the results for unstable coupling between the aileron control mode and antisymmetrical wing torsion mode are plotted including the intervals caused by mass ranges.

nominal	mass of control surfaces			
freq_nom.	freq_low	freq_up	dfreq_low	dfreq_up
[Hz]	[Hz]	[Hz]	[%]	[%]
0.001	0.00	0.00		
0.001	0.00	0.00		
0.001	0.00	0.00		
0.001	0.18	0.19		
0.001	0.05	0.05		
0.001	0.11	0.11		
2.41	2.41	2.41	0.0	0.0
2.82	2.82	2.82	0.0	0.0
6.76	6.76	6.77	0.0	0.1
7.99	7.71	8.31	-3.5	4.0
8.84	8.70	8.99	-1.6	1.7
10.69	10.35	11.07	-3.2	3.6
12.67	12.19	13.20	-3.8	4.1
13.04	12.93	13.15	-0.9	0.8
13.61	13.53	13.70	-0.6	0.7
15.26	15.08	15.45	-1.2	1.2
17.04	16.86	17.23	-1.1	1.1
17.85	17.34	18.41	-2.9	3.1
18.51	17.99	19.07	-2.8	3.0
19.59	18.85	20.41	-3.8	4.2
20.48	19.83	21.18	-3.2	3.4
21.43	20.74	22.19	-3.2	3.5
21.75	21.41	22.11	-1.6	1.7
25.44	25.39	25.50	-0.2	0.2
26.67	26.34	27.01	-1.2	1.3
32.21	32.06	32.35	-0.5	0.4
33.38	32.73	34.08	-1.9	2.1
35.31	34.78	35.87	-1.5	1.6
36.66	36.33	36.99	-0.9	0.9
38.78	37.40	40.32	-3.6	4.0
39.45	38.48	40.50	-2.5	2.7
40.26	39.68	40.87	-1.4	1.5
41.16	40.50	41.86	-1.6	1.7
46.72	45.79	47.70	-2.0	2.1
51.88	50.88	52.95	-1.9	2.1
52.34	51.28	53.46	-2.0	2.1
54.87	54.40	55.35	-0.9	0.9
58.25	54.35	63.14	-6.7	8.4
60.23	56.62	64.63	-6.0	7.3
69.12	66.51	72.05	-3.8	4.2

Table 2, intervals of eigenfrequencies +/-20% mass variation of controls surfaces

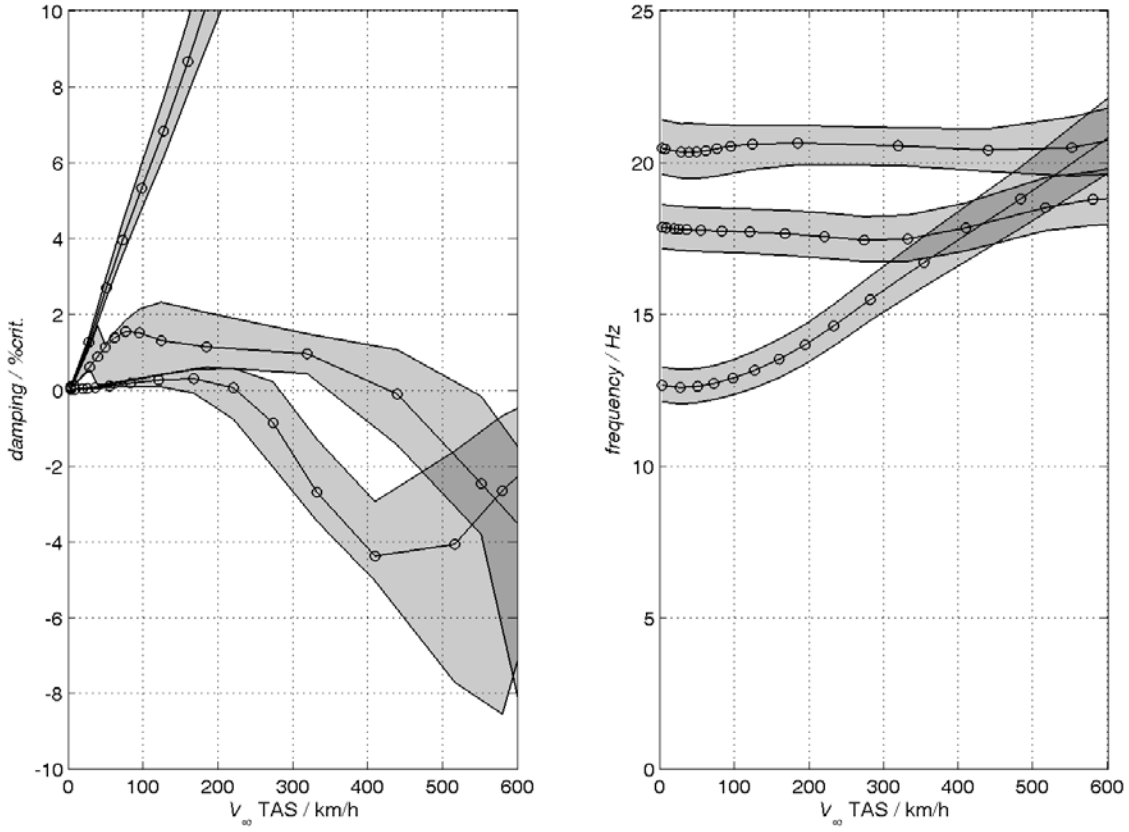

Figure 15, rudder mode and antisymmetric empennage bending, with +/-20% tolerance in rudder mass

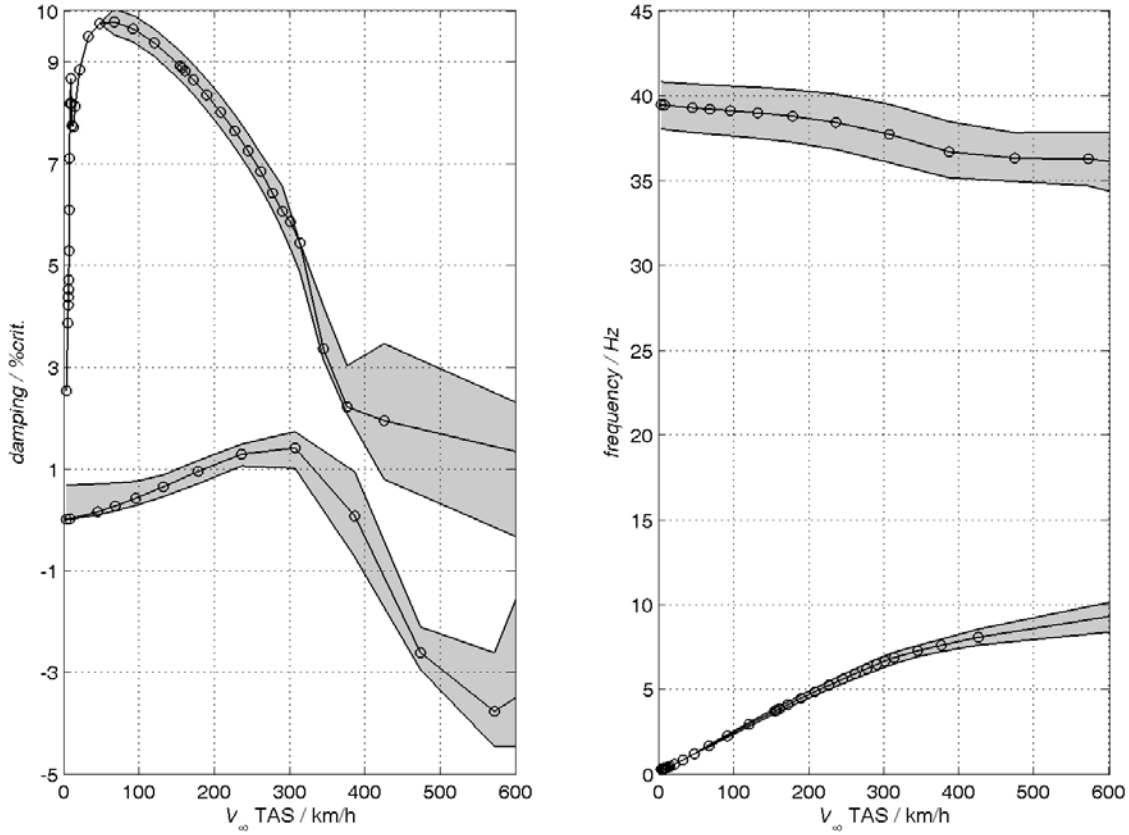

Figure 16, aileron control mode and antisymmetric wing torsion, with +/-20% tolerance in aileron mass

6.4 I23 Flutter results including GVT measurement errors

In the GVT report of the I23 data regarding the accuracy of measurements are summarized:

uncertainty of resonance frequency	1.0%
uncertainty of accelerometer calibration at 20 Hz	1.8%
uncertainty of amplitude measurements in range 5 -100 Hz	3.0%
uncertainty of accelerometer linearity	1.0%
uncertainty of voltage measurements and calculations	0.5%

complex standard uncertainty for acceleration measurements:

$$\varepsilon = \sqrt{0.018^2 + 0.03^2 + 0.01^2 + 0.005^2} = 0.037$$

total uncertainty in acceleration amplitude: 3.7% of measured value

To evaluate the influence of measurement accuracy in GVT for the flutter stability results, these uncertainty ranges were introduced in the interval flutter analysis. In Figure 17 the resulting uncertainty bands of all damping and frequency curves excluding the rigid body modes are plotted.

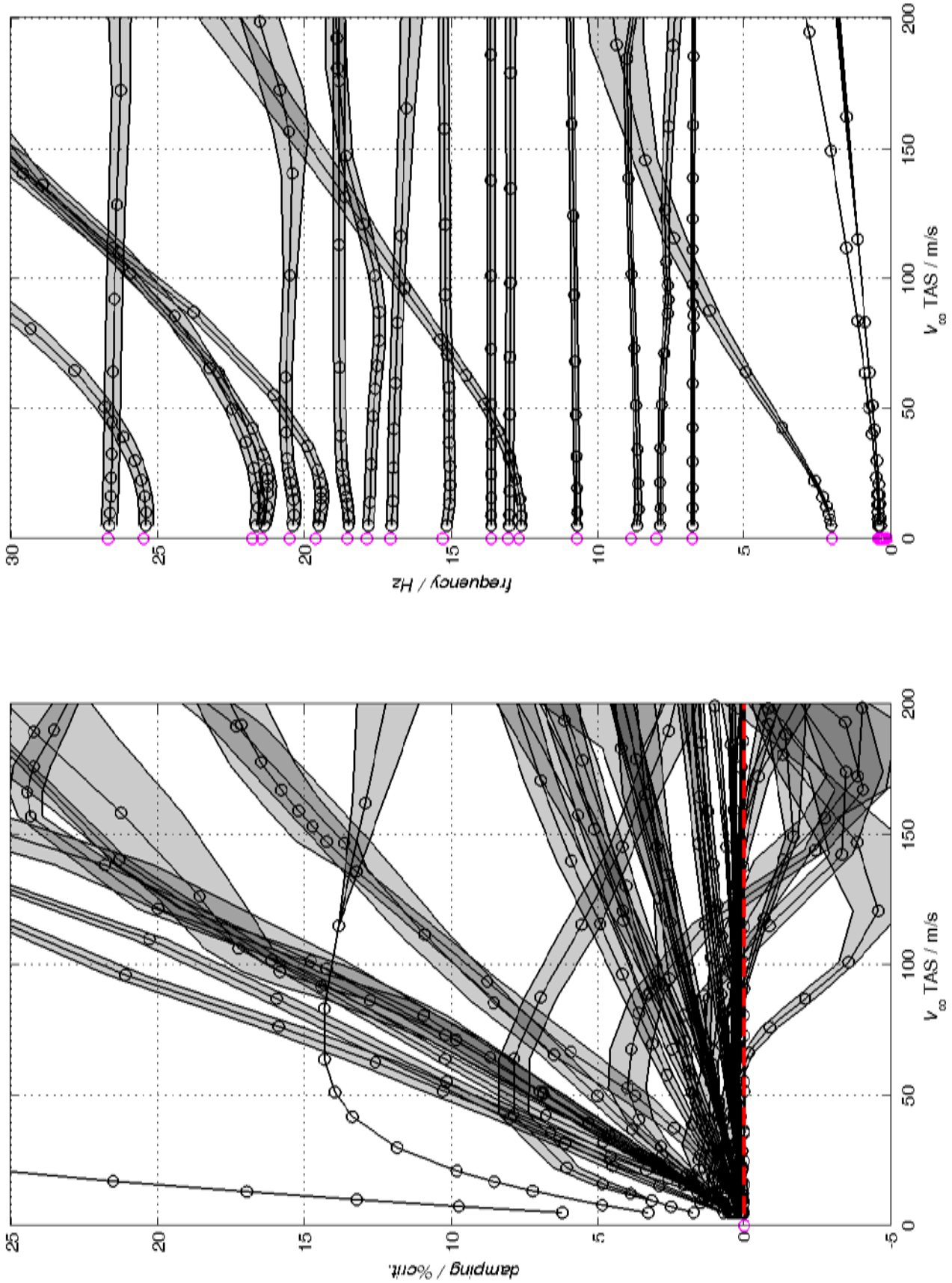

Figure 17, flutter results including typical measurement errors in GVT

7 Conclusions

The robust analysis of the flutter stability of aircraft requires a consideration of effects resulting structural uncertainties. These uncertainties are related to production tolerances and variations in material characteristics, or to necessary simplifications of the numerical model used for the simulation. The characteristics may be formulated in intervals with lower and upper bounds of eigen frequencies and mode shapes, which are determined using the interval modal analysis presented in this report. The uncertainties are propagated through the flutter analysis by application of the continuation method. The aeroelastic stability of the nominal aircraft is analyzed with increasing flight velocity using a predictor-corrector technique. At every intermediate velocity step, the perturbed flutter equations are solved for the bounds resulting from modal intervals by sensitivity evalauation. It is shown that the presented interval flutter analysis method calculates conservative confidence intervals of dampings and frequencies for bounded but uncertain structural parameters in critical ranges.

8 References

[1] Albano, E.; Rodden, W. P.; A Doublet-Lattice Method for Calculating Lift Distributions on Oscillating Surfaces in Subsonic Flows. AIAA Journal, Vol. 7 (1969) No. 2, pp. 279-285.

[2] van Zyl, L.; Robustness of the subsonic doublet lattice method. Aeronautical Journal, Vol. 107 (2003) No. 2, pp. 257-262.

[3] Balmes, E.; Parametric families of reduced finite element models. Theory and applications. Mechanical Systems and Signal Processing, Vol. 10 (1996), No. 4, pp. 381–394, 1996.

[4] Balmes, E.: Optimal Ritz Vectors for Component Mode Synthesis Using the Singular Value Decomposition. AIAA Journal, Vol. 34 (1996) No. 6, pp. 1256-1260.

[5] Borglund, D.; The µ-k Method for Robust Flutter Solutions. Journal of Aircraft, Vol. 41 (2004) No. 5, pp. 1209-1216.

[6] Cardani, C.; Mantegazza, P.; Continuation and Direct Solution of the Flutter Equation. Computers & Structures, Vol. 8 (1978) No. 3, pp. 185-192.

[7] Chen, P. C.; A Damping Perturbation Method for Flutter Solution: the g-Method. AIAA Journal Vol. 38 (2000) No. 9, pp. 1519-1524.

[8] Deif, S.; The interval eigenvalue problem. Zeitschrift für Angewandte Mathematik und Mechanik, No. 71, pp. 61-64.

[9] Dhooge, A.; Govaerts, W.; Kuznetsov, Y.A.: Cl_MATCONT: A Continuation Toolbox in Matlab. Proceedings of the 2003 ACM Symposium on Applied Computing (SAC), Melbourne, FL, USA, March 9-12, 2003.

[10] Fox, R.L.; Kapoor, M.P.; Rates of Change of Eigenvalues and Eigenvectors. AIAA Journal Vol. 16 (1968) No. 12, pp. 2426–2429.

[11] Hassig, H.; An Approximate True Damping Solution of the Flutter Equation by Determinant Iteration. Journal of Aircraft, Vol.8 (1971) No. 11, pp. 885-889.

[12] Lind, R.; and Brenner; M.: Robust Aeroservoelastic Stability Analysis, Springer–Verlag, London, 1999.

[13] Kiessling, F.; Potkanski W.; Nonlinear Flutter Analysis by a Continuation Method. Proc. 2nd International Conference EAHE Engineering Aero-Hydroelasticity, Pilsen, June 6-10, 1994, pp. 221-226.

[14] Kreinovich, V.; Beck, J.; Monte-Carlo-Type Techniques for Processing Interval Uncertainty, and Their Potential Engineering Applications. Reliable Computing, Vol. 13 (2007) No. 1, pp. 25-69.

[15] Meyer, E. E.; Application of a New Continuation Method to Flutter Equations. 29th Structures, Structural Dynamics and Materials Conference, April 18-20,

1988, Williamsburg, VA, Part 3, pp.1118-1123.

[16] Moens D.; Vandepitte, D.; A survey of non-probabilistic uncertainty treatment in finite element analysis. Computer Methods in Applied Mechanics and Engineering, Vol. 194, Issues 12-16, 8 April 2005, pp. 1527-1555.

[17] Sim, J., Qiu, Z., Wanga, X.; Modal analysis of structures with uncertain-but-bounded parameters via interval analysis. Journal of Sound and Vibration. Vol. 303, Issues 1-2, June 2007, pp. 29-45.

[18] N. N.; ZAERO Version 7.3 Theoretical Manual, ZONA 02-12.4, ZONA Technology Inc., 2005.

[19] N. N.; MSC.NASTRAN Aeroelastic Analysis Users' Guide V68. MSC Software Corporation, 2004.

[20] Chajec, W.; Aeroelastic Reference Model of I-23 - Flutter Calculation Based on GVT Results. EU-project Cost-Effective Small AiRcraft CESAR founded by European Commision, Contract no: AIP5-CT-2006-030888.

[21] Schwochow, J.; Interpolation of GVT Results using Volume-Spline Method. EU-project Cost-Effective Small AiRcraft CESAR founded by European Commision, Contract no: AIP5-CT-2006-030888.

9 Appendix A – I23 geometry

External dimensions – View in three projection

(The dimensions are specified in millimeters)

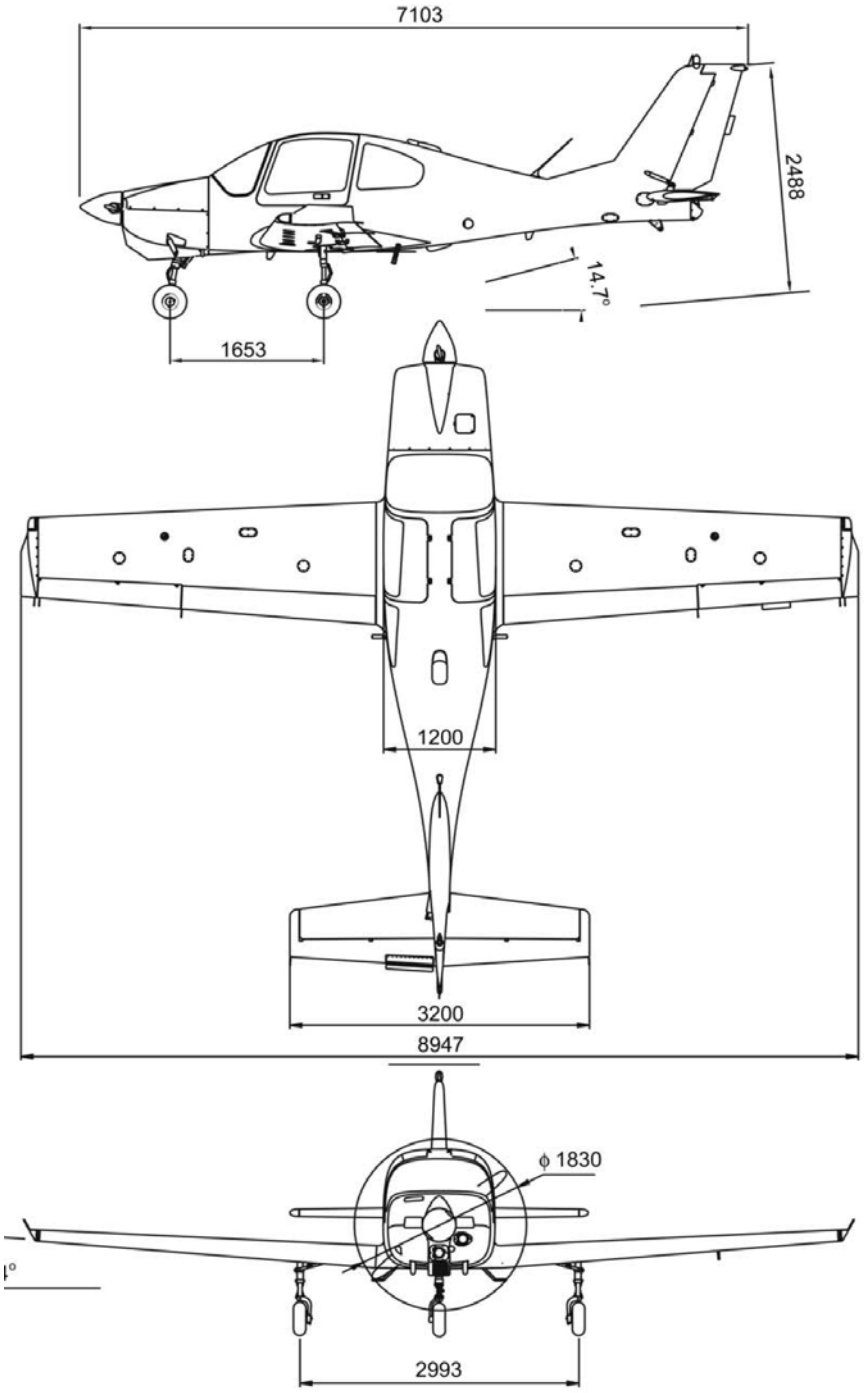

Figure 18, I23 geometry definition

10 Appendix B – I23 modal parameter

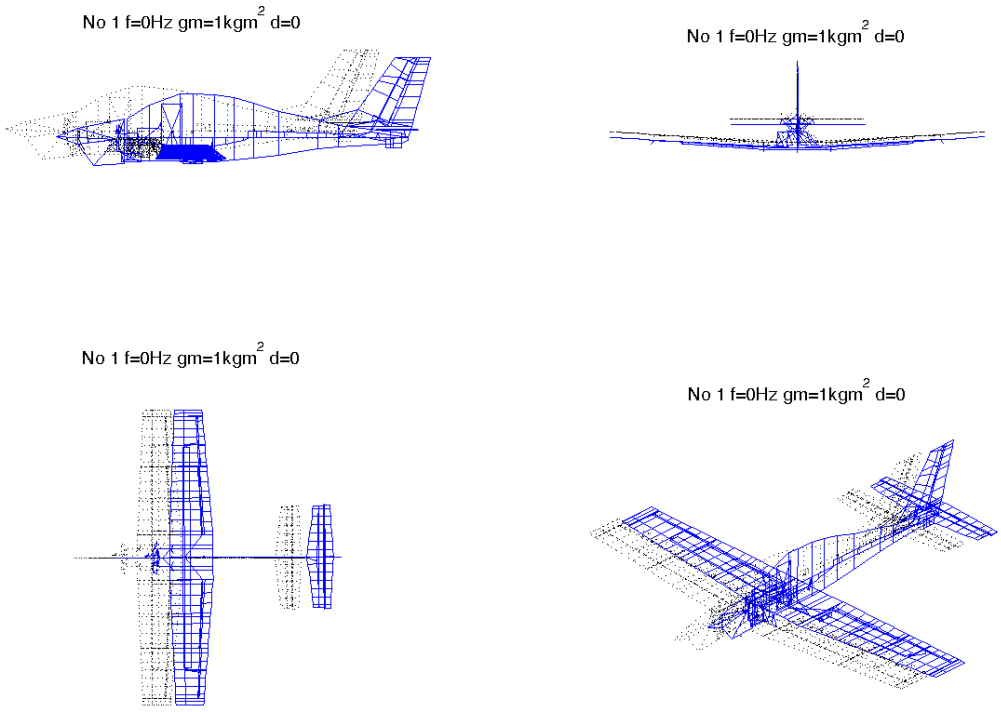

Mode 1: form: 1, f = 0.00 Hz, gm = 1.0 kgm², d = 0.00 %crit.

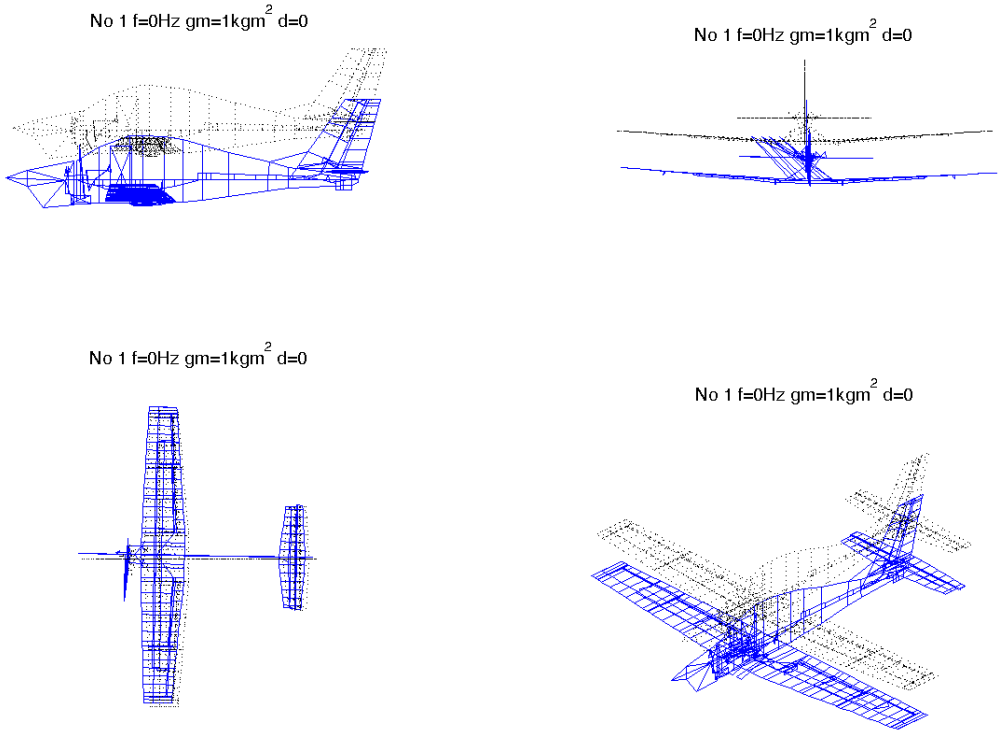

Mode 2: form: 2, f = 0.00 Hz, gm = 1.0 kgm², d = 0.00 %crit.

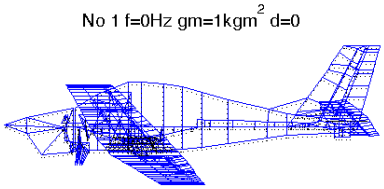

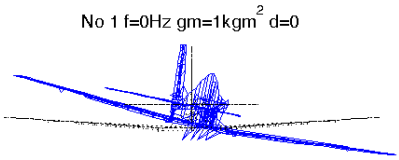

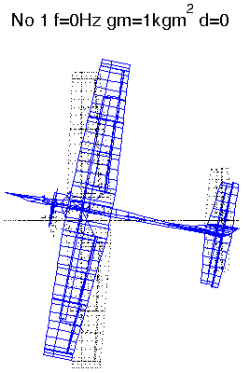

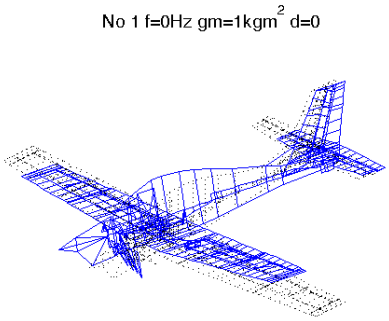

Mode 3: form: 3, f = 0.00 Hz, gm = 1.0 kgm², d = 0.00 %crit.

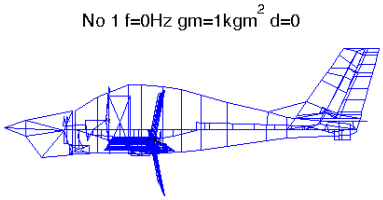

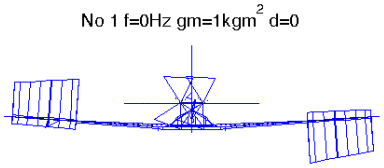

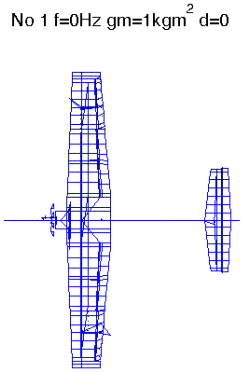

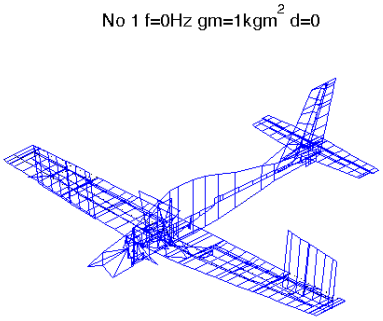

Mode 4: form: 4, f = 0.00 Hz, gm = 1.0 kgm², d = 0.00 %crit.

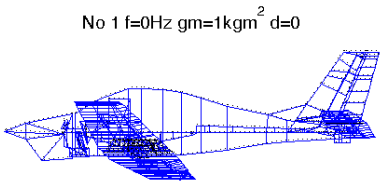

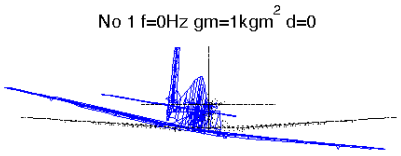

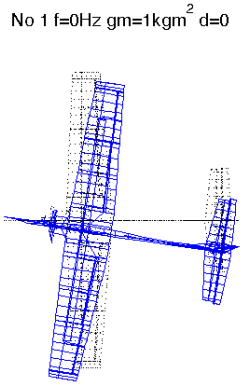

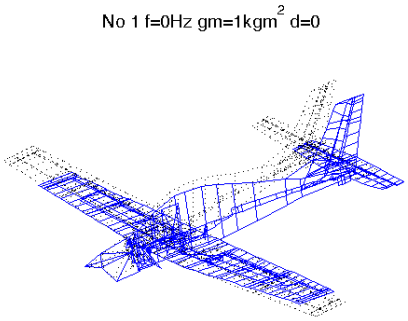

Mode 5: form: 5, f = 0.00 Hz, gm = 1.0 kgm², d = 0.00 %crit.

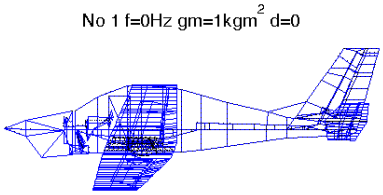

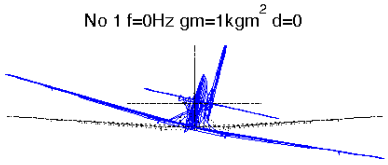

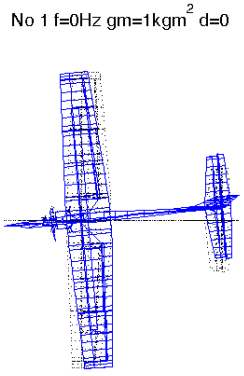

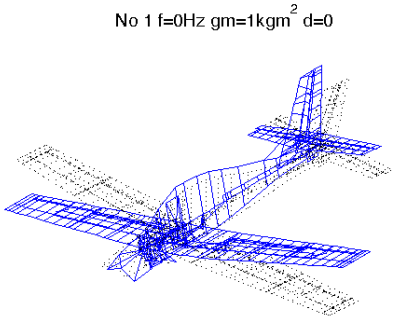

Mode 6: form: 6, f = 0.00 Hz, gm = 1.0 kgm², d = 0.00 %crit.

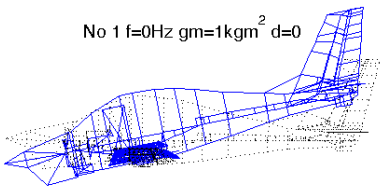

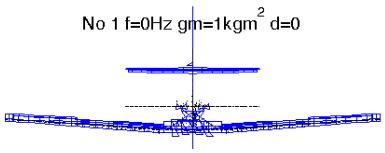

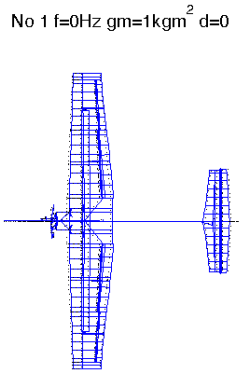

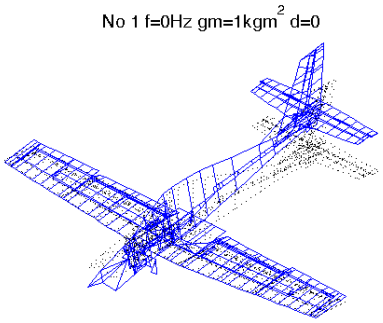

Mode 7: form: 7, f = 0.00 Hz, gm = 1.0 kgm², d = 0.00 %crit.

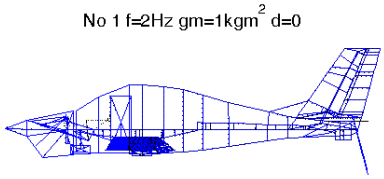

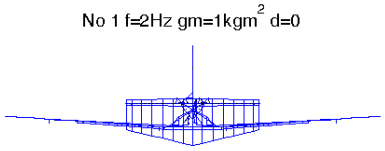

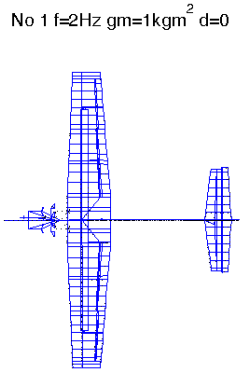

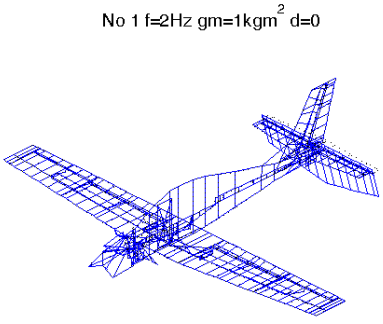

Mode 8: form: 8, f = 2.00 Hz, gm = 1.0 kgm², d = 0.00 %crit.

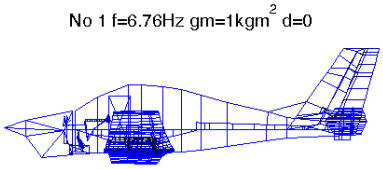

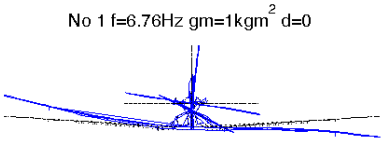

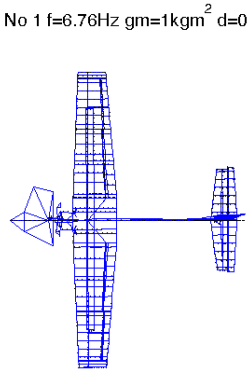

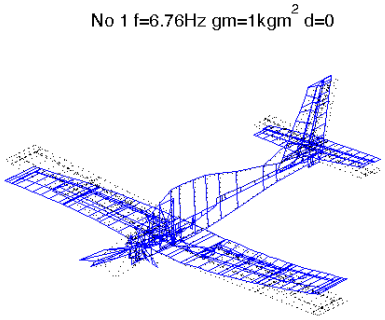

Mode 9: form: 9, f = 6.76 Hz, gm = 1.0 kgm², d = 0.00 %crit.

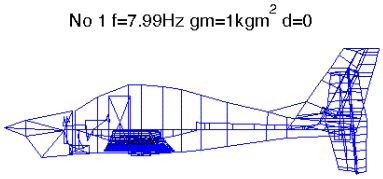

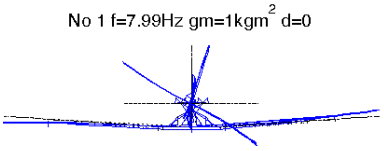

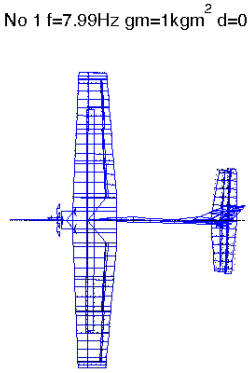

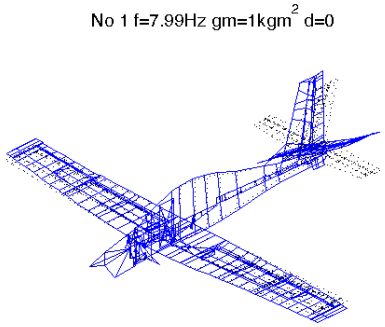

Mode 10: form: 10, f = 7.99 Hz, gm = 1.0 kgm², d = 0.00 %crit.

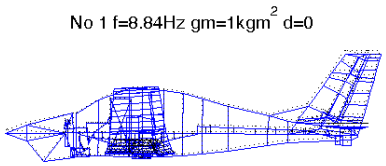

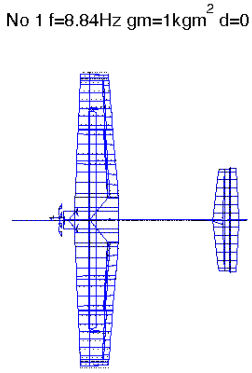

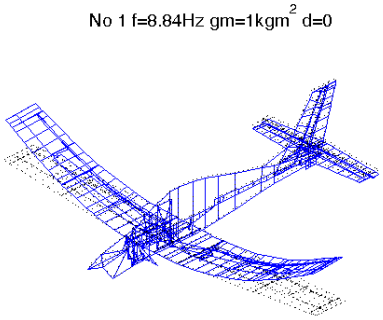

Mode 11: form: 11, f = 8.84 Hz, gm = 1.0 kgm², d = 0.00 %crit.

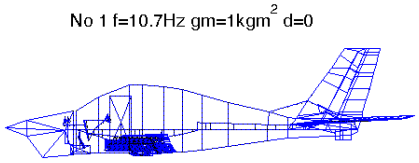

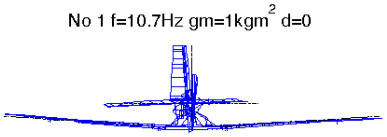

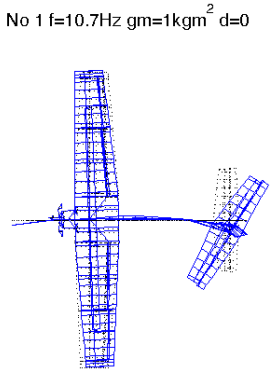

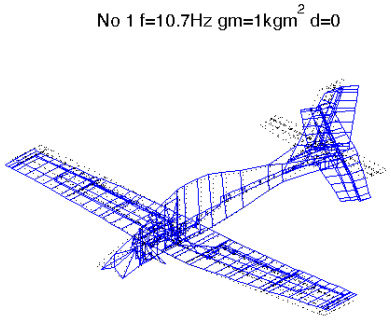

Mode 12: form: 12, f = 10.69 Hz, gm = 1.0 kgm², d = 0.00 %crit.

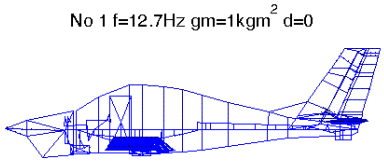

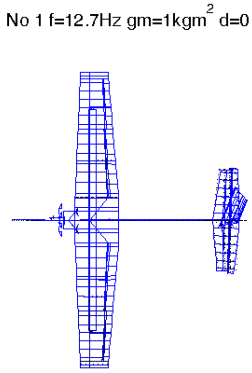

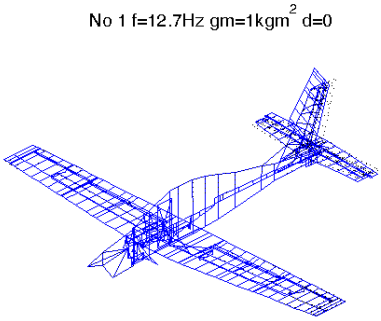

Mode 13: form: 13, f = 12.67 Hz, gm = 1.0 kgm², d = 0.00 %crit.

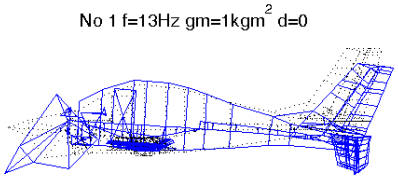

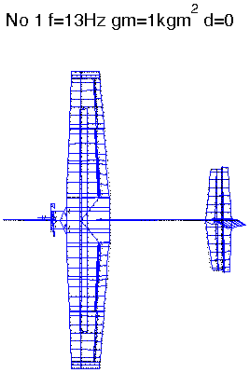

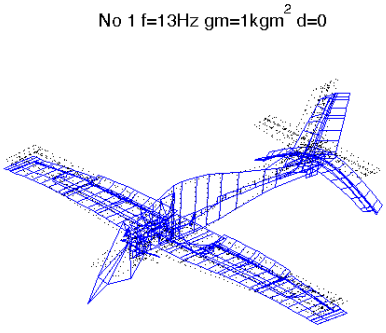

Mode 14: form: 14, f = 13.04 Hz, gm = 1.0 kgm², d = 0.00 %crit.

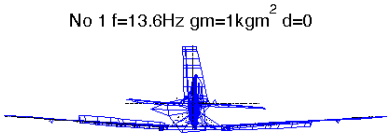

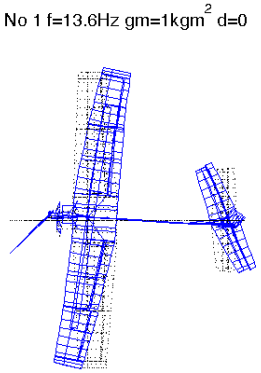

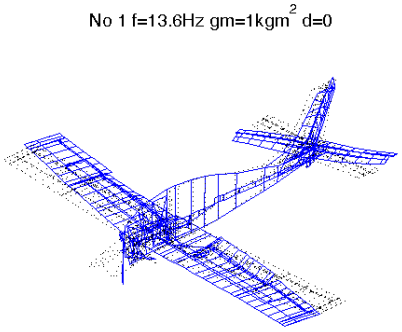

Mode 15: form: 15, f = 13.61 Hz, gm = 1.0 kgm², d = 0.00 %crit.

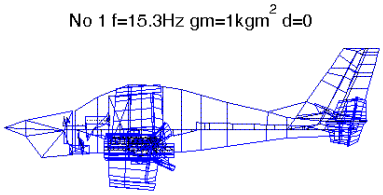

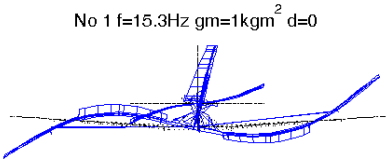

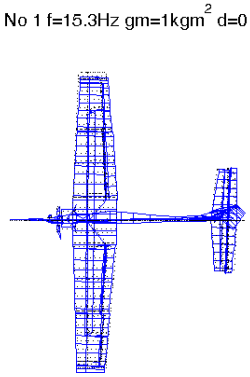

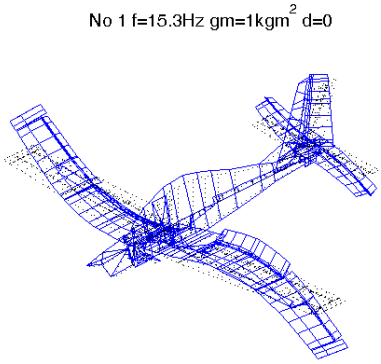

Mode 16: form: 16, f = 15.26 Hz, gm = 1.0 kgm², d = 0.00 %crit.

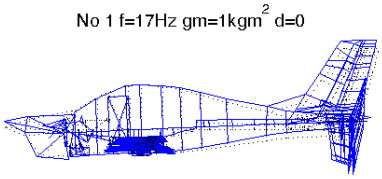

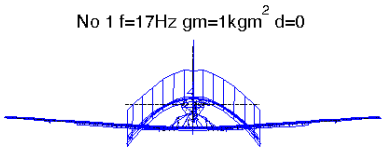

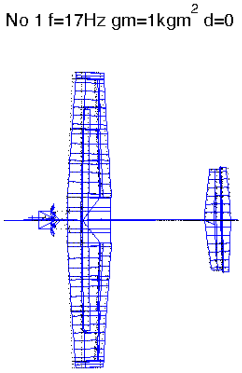

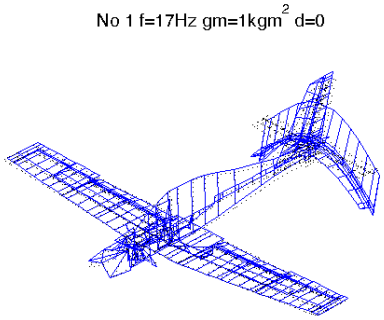

Mode 17: form: 17, f = 17.04 Hz, gm = 1.0 kgm², d = 0.00 %crit.

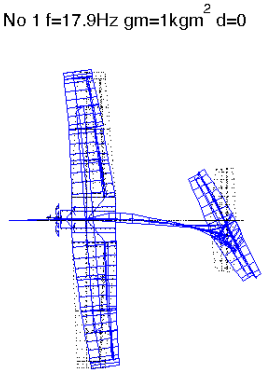

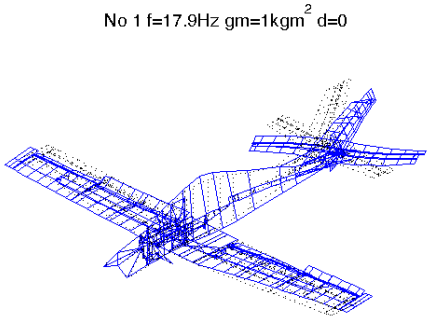

Mode 18: form: 18, f = 17.85 Hz, gm = 1.0 kgm², d = 0.00 %crit.

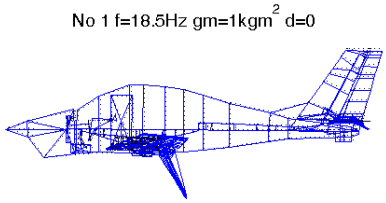

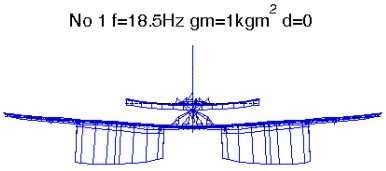

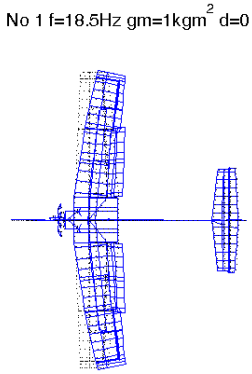

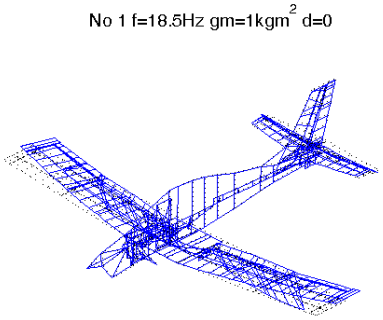

Mode 19: form: 19, f = 18.51 Hz, gm = 1.0 kgm², d = 0.00 %crit.

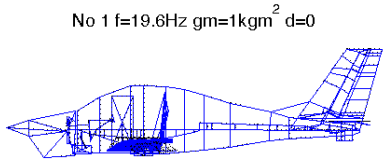

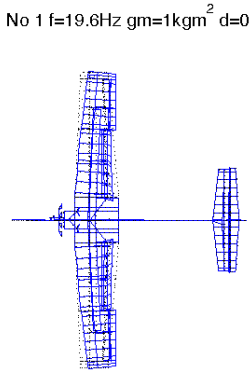

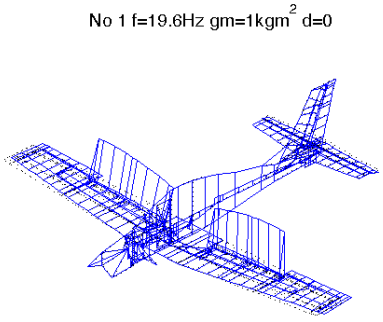

Mode 20: form: 20, f = 19.59 Hz, gm = 1.0 kgm², d = 0.00 %crit.

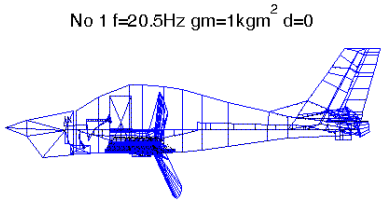

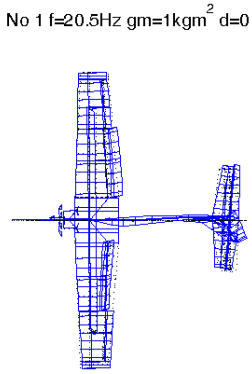

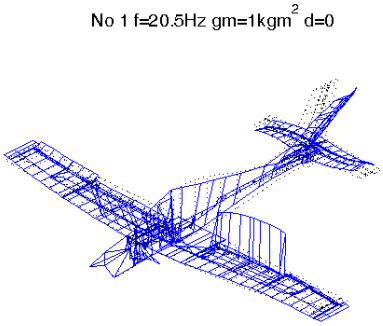

Mode 21: form: 21, f = 20.48 Hz, gm = 1.0 kgm², d = 0.00 %crit.

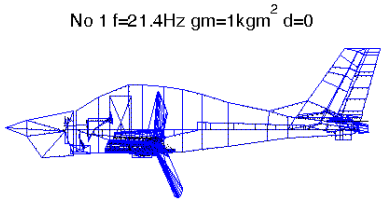

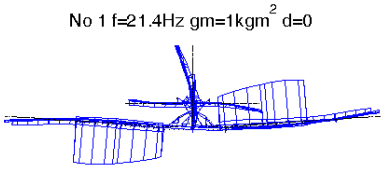

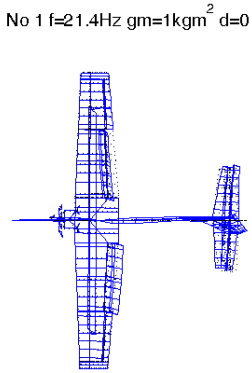

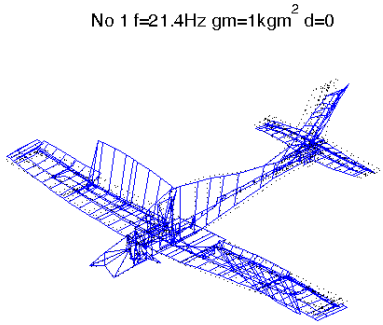

Mode 22: form: 22, f = 21.43 Hz, gm = 1.0 kgm², d = 0.00 %crit.

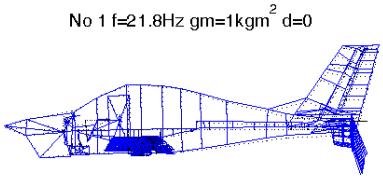

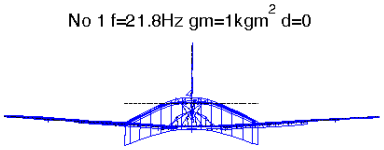

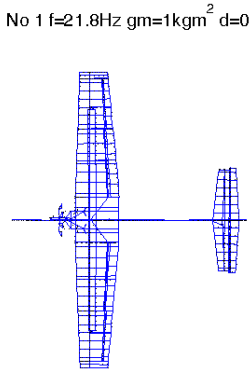

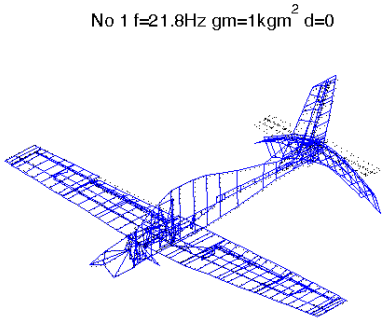

Mode 23: form: 23, f = 21.75 Hz, gm = 1.0 kgm², d = 0.00 %crit.

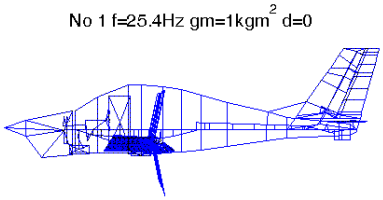

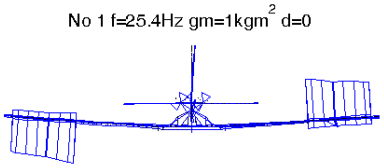

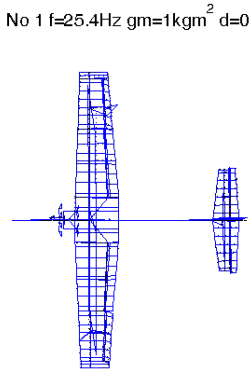

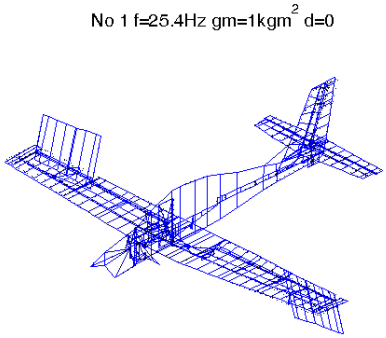

Mode 24: form: 24, f = 25.44 Hz, gm = 1.0 kgm², d = 0.00 %crit.

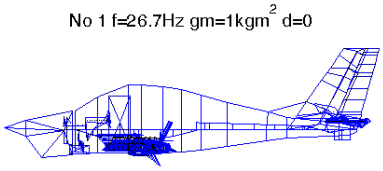

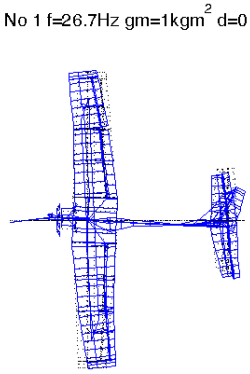

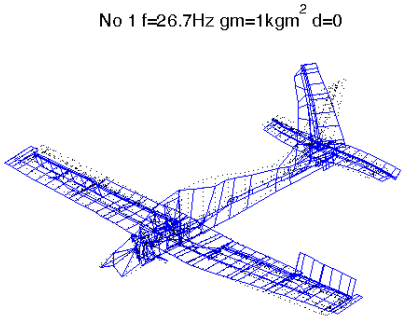

Mode 25: form: 25, f = 26.67 Hz, gm = 1.0 kgm², d = 0.00 %crit.

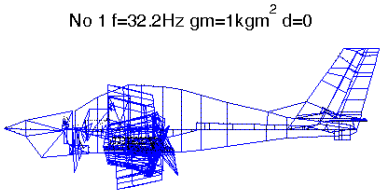

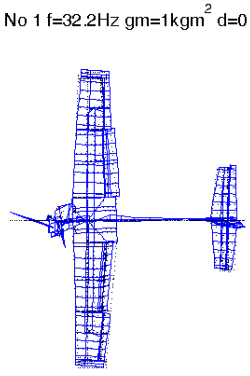

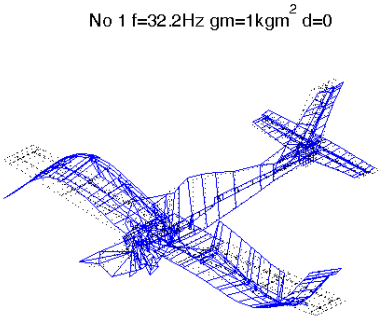

Mode 26: form: 26, f = 32.21 Hz, gm = 1.0 kgm², d = 0.00 %crit.

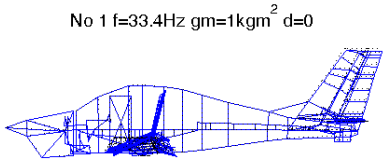

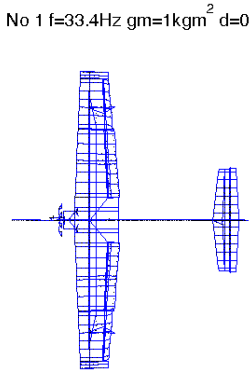

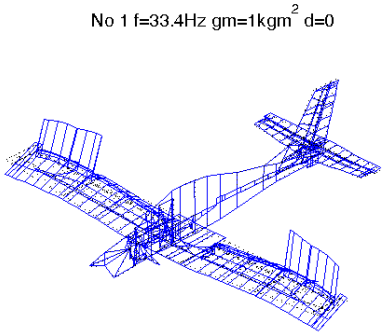

Mode 27: form: 27, f = 33.38 Hz, gm = 1.0 kgm², d = 0.00 %crit.

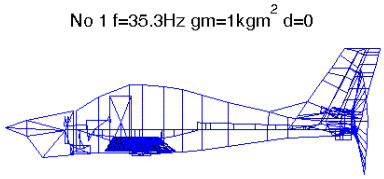

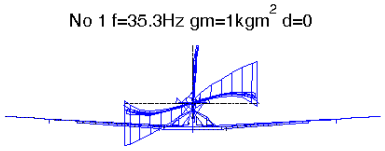

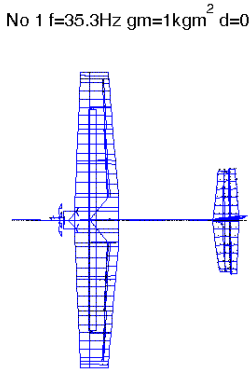

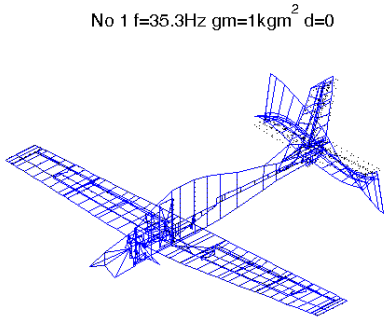

Mode 28: form: 28, f = 35.31 Hz, gm = 1.0 kgm², d = 0.00 %crit.

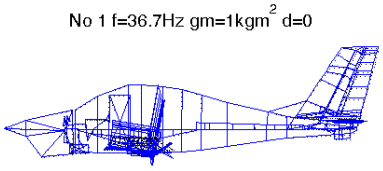

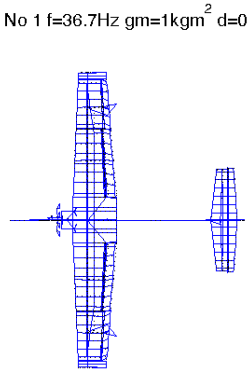

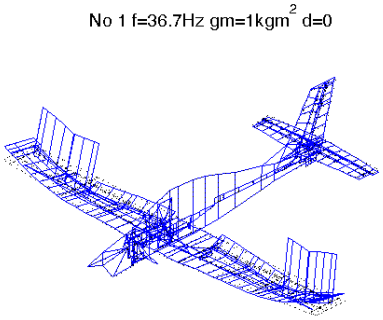

Mode 29: form: 29, f = 36.66 Hz, gm = 1.0 kgm², d = 0.00 %crit.

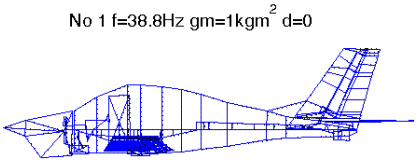

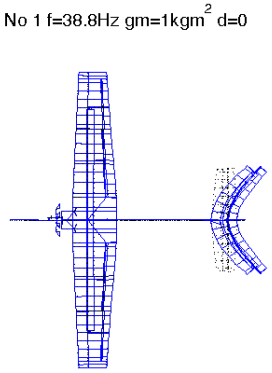

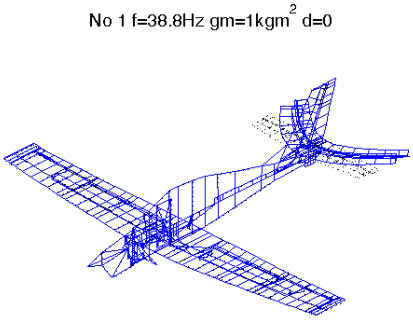

Mode 30: form: 30, f = 38.78 Hz, gm = 1.0 kgm², d = 0.00 %crit.

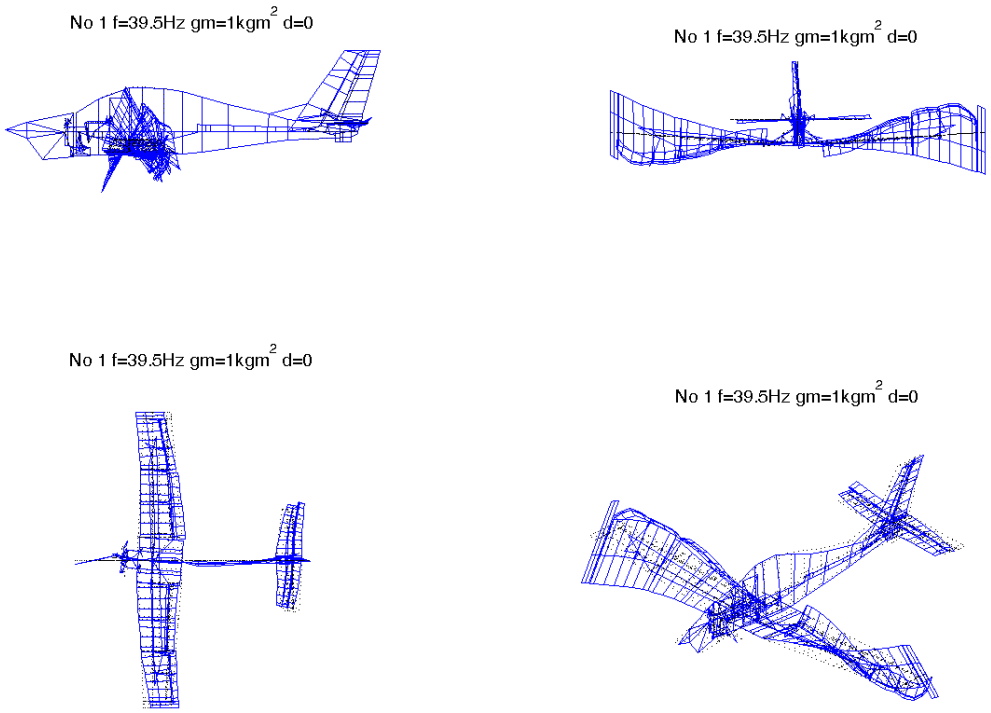

Mode 31: form: 31, f = 39.45 Hz, gm = 1.0 kgm², d = 0.00 %crit.

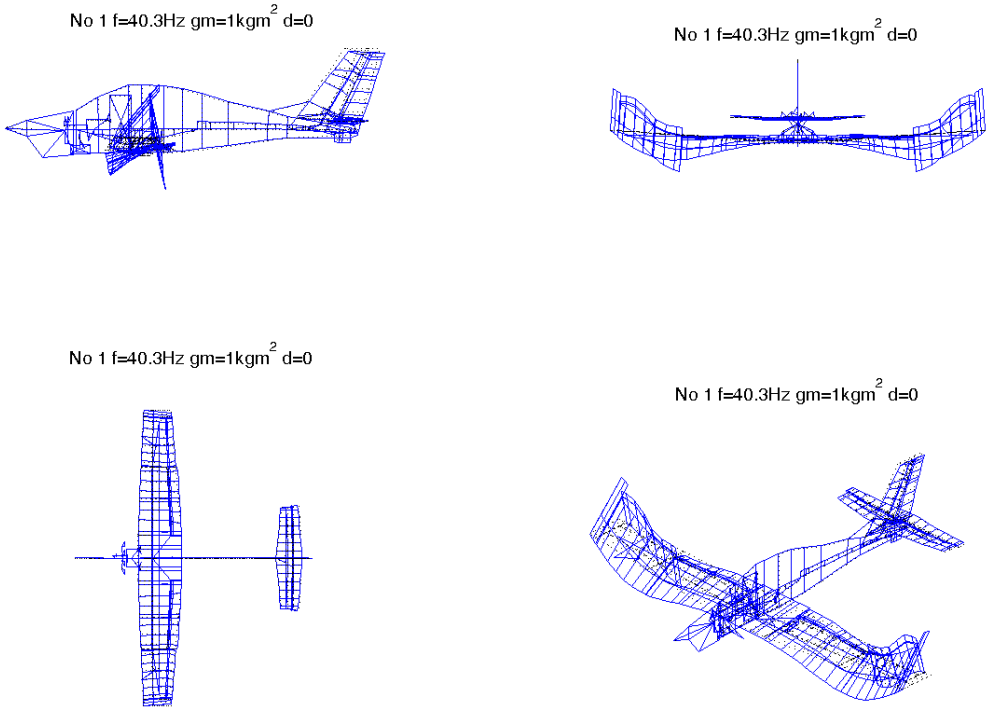

Mode 32: form: 32, f = 40.26 Hz, gm = 1.0 kgm², d = 0.00 %crit.

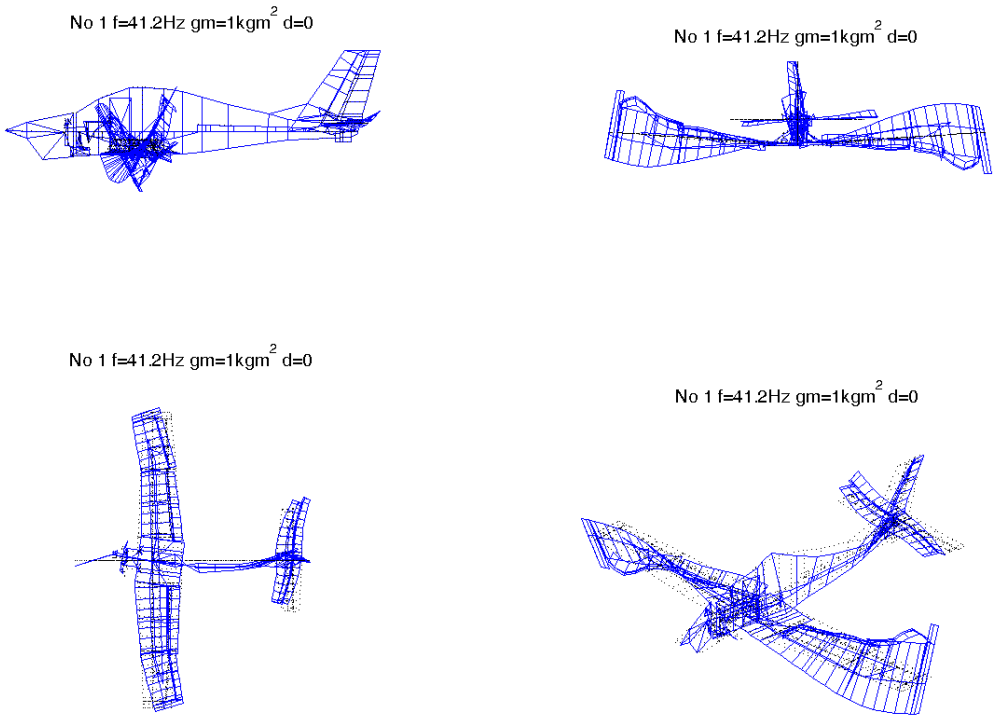

Mode 33: form: 33, f = 41.16 Hz, gm = 1.0 kgm², d = 0.00 %crit.

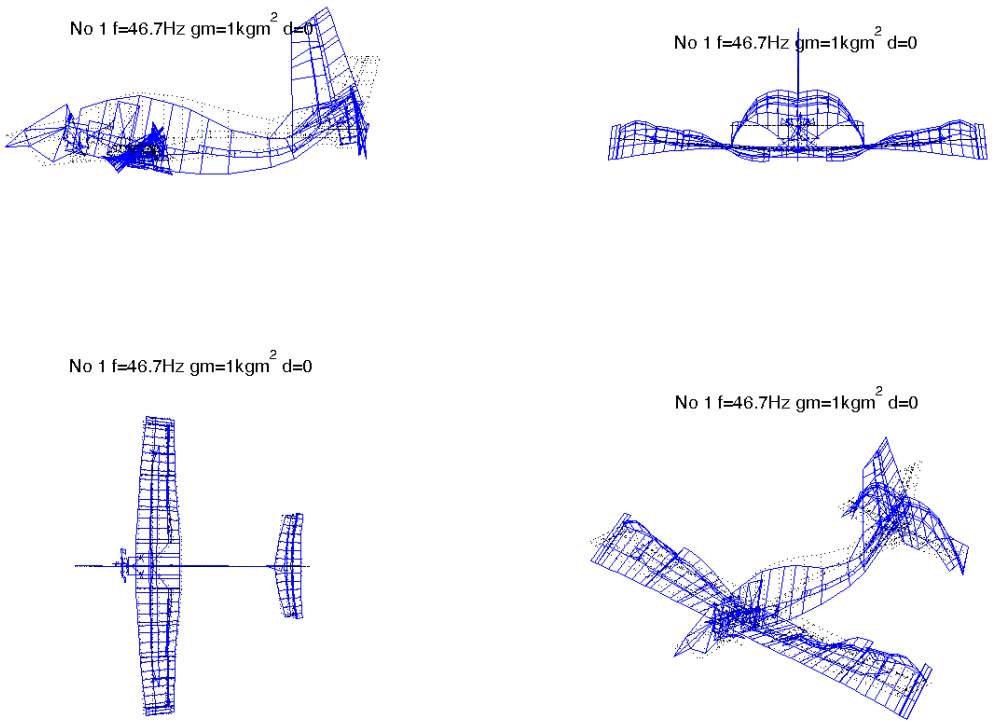

Mode 34: form: 34, f = 46.72 Hz, gm = 1.0 kgm², d = 0.00 %crit.

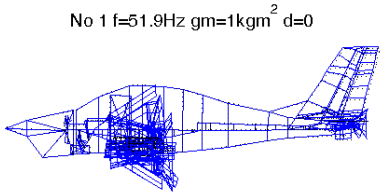

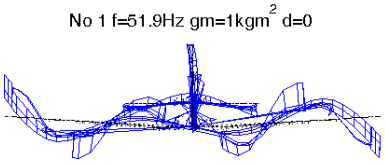

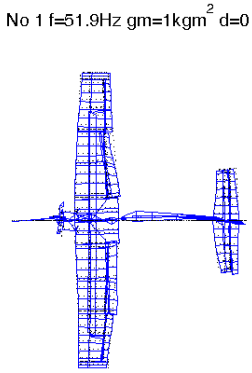

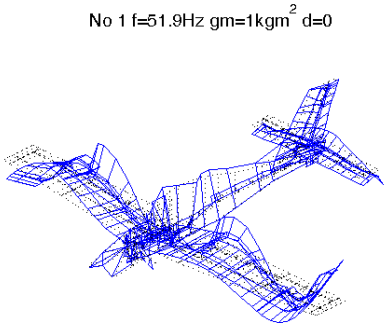

Mode 35: form: 35, f = 51.88 Hz, gm = 1.0 kgm², d = 0.00 %crit.

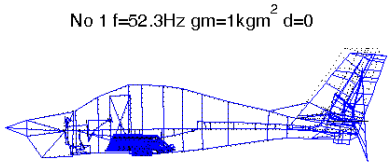

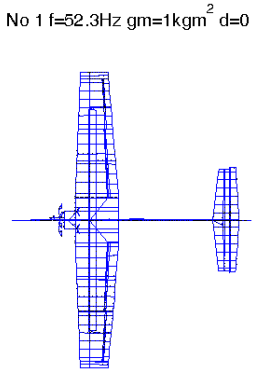

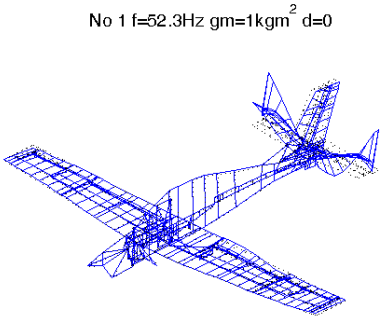

Mode 36: form: 36, f = 52.34 Hz, gm = 1.0 kgm², d = 0.00 %crit.

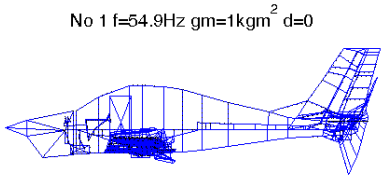

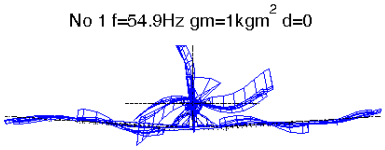

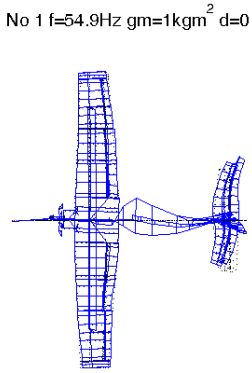

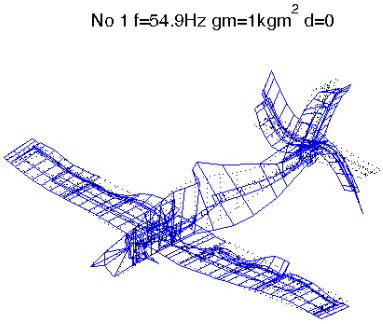

Mode 37: form: 37, f = 54.87 Hz, gm = 1.0 kgm², d = 0.00 %crit.

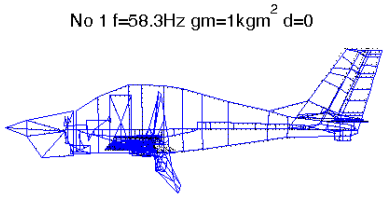

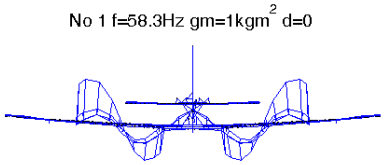

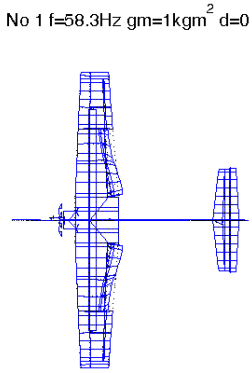

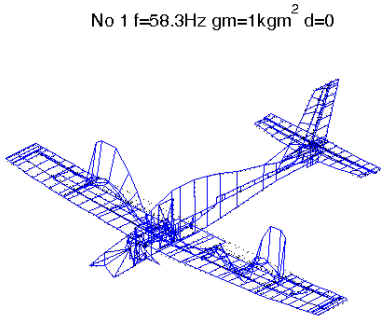

Mode 38: form: 38, f = 58.25 Hz, gm = 1.0 kgm², d = 0.00 %crit.

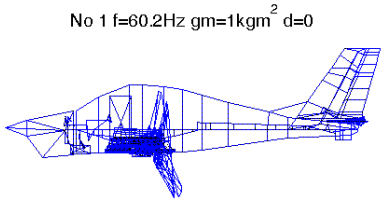

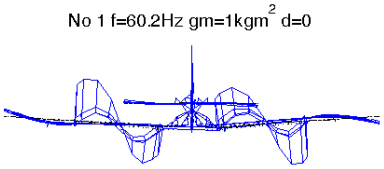

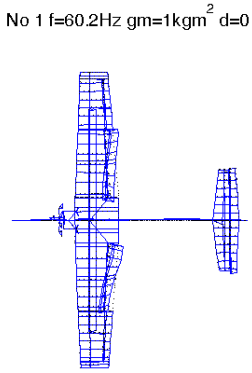

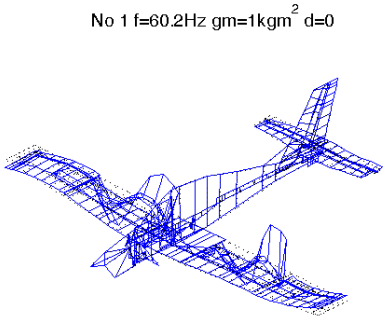

Mode 39: form: 39, f = 60.23 Hz, gm = 1.0 kgm², d = 0.00 %crit.

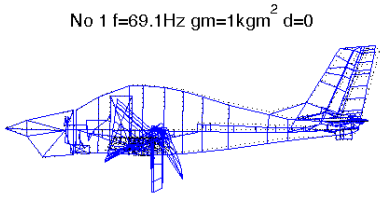

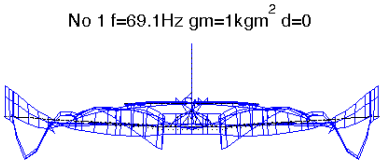

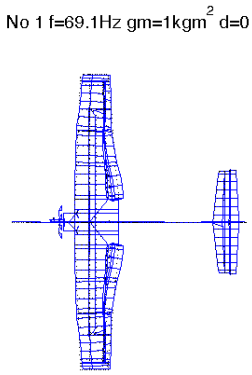

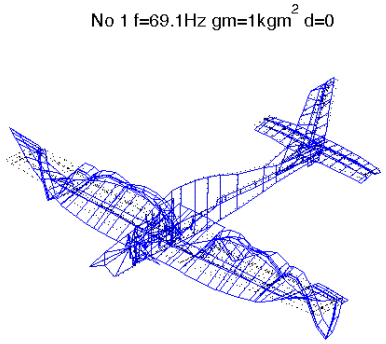

Mode 40: form: 40, f = 69.12 Hz, gm = 1.0 kgm², d = 0.00 %crit.